MICROBIOLOGY

A secreted sirtuin from *Campylobacter jejuni* contributes to neutrophil activation and intestinal inflammation during infection

Sean M. Callahan[1], Trevor J. Hancock[1,2], Ryan S. Doster[3,4]†, Caroline B. Parker[1], Mary E. Wakim[1]‡, Jennifer A. Gaddy[3], Jeremiah G. Johnson[1]*

Histone modifications control numerous processes in eukaryotes, including inflammation. Some bacterial pathogens alter the activity or expression of host-derived factors, including sirtuins, to modify histones and induce responses that promote infection. In this study, we identified a deacetylase encoded by *Campylobacter jejuni* which has sirtuin activities and contributes to activation of human neutrophils by the pathogen. This sirtuin is secreted from the bacterium into neutrophils, where it associates with and deacetylates host histones to promote neutrophil activation and extracellular trap production. Using the murine model of campylobacteriosis, we found that a mutant of this bacterial sirtuin efficiently colonized the gastrointestinal tract but was unable to induce cytokine production, gastrointestinal inflammation, and tissue pathology. In conclusion, these results suggest that secreted bacterial sirtuins represent a previously unreported class of bacterial effector and that bacterial-mediated modification of host histones is responsible for the inflammation and pathology that occurs during campylobacteriosis.

INTRODUCTION

Campylobacter species are a leading cause of bacterial-derived gastroenteritis worldwide, infecting a projected ninety million individuals (*1*, *2*). While infection is often self-limiting in immunocompetent individuals, numerous postinfectious disorders can develop, including Guillain-Barré syndrome, irritable bowel syndrome, and reactive arthritis (*3*, *4*). In addition to the prevalence of infection and these various outcomes, the high incidence of antibiotic resistance has led both the Centers for Disease Control and World Health Organization to classify *Campylobacter* spp. as serious threats to public health (*5*, *6*). Despite these impacts, little is known about which bacterial and host factors are responsible for the inflammation that occurs during human campylobacteriosis and how that might be responsible for intestinal disease. In our previous work, we found that neutrophils are recruited to the site of infection and that predominantly neutrophil-derived proteins are present in fecal samples of *Campylobacter jejuni*–infected patients. In addition, we found that *C. jejuni* is a potent activator of human neutrophils and that stimulation leads to the production of neutrophil extracellular traps (NETs), which appear to localize to abscesses within colonic crypts (*7*, *8*). Because neutrophil activation during campylobacteriosis has been associated with inflammation and tissue pathology (*9*–*11*), understanding the microbial factors that drive activation and NET production could lead to the development of novel therapeutics. Unfortunately, little data exist as to how neutrophils are activated and are induced to elicit such a proinflammatory response such as the production of NETs.

One explanation for how *Campylobacter* spp. activate and promote inflammatory responses from neutrophils is through impacts to the posttranslational modifications (PTMs) on neutrophil proteins, which have been shown to play a vital role in orchestrating host-microbe interactions within eukaryotes. For example, differential acetylation of host proteins is accomplished using numerous enzymes, including histone acetyltransferases (HATs) and histone deacetylases (HDACs), the outcomes of which affect processes involved in autoimmunity, inflammation, and tumorigenesis (*12*–*14*). Because the host uses acetylation to control these cellular processes, pathogens such as *Listeria monocytogenes*, *Salmonella typhimurium*, and *Mycobacterium tuberculosis* have evolved to manipulate and use host-derived HATs and HDACs to promote infection, especially sirtuin-2 (SIRT2) (*15*–*21*). In addition, other research has shown that some bacterial-derived effectors can directly affect host PTMs and that these enzymes may have been acquired from the host and incorporated into pathogen's virulence factor repertoire or convergently evolved to mimic the activity of host enzymes (*22*–*24*). Bacterial effectors that are translocated and directly bind host proteins to differentially acetylate them remain to be identified.

In eukaryotes, a common target of PTMs is histones, which play a critical role in the structure and function of chromatin, which can have profound effects on gene expression. Core histones are characterized by a histone folding domain and N-terminal tails accessible to enzymes involved in PTMs (*25*). For example, HATs acetylate the ε-amino group of lysine residues on histones, which results in a neutral charge and opening of chromatin for RNA polymerase (*26*). In contrast, during histone deacetylation, the acetyl group is removed from lysine residues, which causes the chromatin to close and prevent RNA polymerase binding (*27*). Beyond reducing transcription, other research found that HDACs can induce gene

[1]Department of Microbiology, University of Tennessee, Knoxville, TN 37996, USA. [2]Department of Medicine, University of Tennessee Medical Center, Knoxville, TN 37930, USA. [3]Division of Infectious Diseases, Department of Medicine Vanderbilt University Medical Center, Nashville, TN 37232, USA. [4]Department of Microbiology and Immunology, University of Louisville, Louisville, KY 40202, USA.
*Corresponding author. Email: jjohn358@utk.edu
†Clinical and Translational Research Building, Room 605, University of Louisville, 505 South Hancock Street, Louisville, KY 40202, USA.
‡Department of Microbiology, Immunology, and Cancer Biology, University of Virginia, Charlottesville, VA 22908, USA.

expression by limiting acetylation near gene bodies and intergenic regions, which allows RNA elongation factors to bind more readily (*28*–*30*). As a result, numerous proinflammatory genes are up-regulated in response to HDAC activity, including interleukin-8 (IL-8), colony-stimulating factor–1, and tumor necrosis factor–α (TNF-α) (*31*–*33*).

In addition to affecting gene expression, differential acetylation of proteins, including histones, can alter other cellular responses. In neutrophils, for example, increased HDAC activity promotes citrullination of histone H3 by protein arginine deiminase 4 (PAD4), which results in the elaboration of NETs and the associated inflammation (*34*–*36*). This posttranslational conversion of arginine to citrulline on histone H3 through PAD4 replaces the primary ketamide with a ketone group and is indispensable in the production of NETs (*37*). Further, PAD4 promotes decondensation of heterochromatin to facilitate NET release into the extracellular milieu (*38*). Despite the apparent relation between histone acetylation and neutrophil physiology, the role of sirtuins in these responses is not well defined.

Because histone acetylation plays a role in proinflammatory gene expression and cellular outcomes, investigators have sought to characterize their effects in various diseases and whether altering these responses can improve health. For example, in the healthy gastrointestinal tract, inhibition of deacetylase activity is a naturally occurring phenomenon. For example, butyrate is a short-chain fatty acid produced by the human gut microbiota as a by-product of dietary fiber fermentation (*39*) that binds to and inhibits the activity of various HDACs and sirtuins. Through this inhibitory effect, butyrate has been shown to reduce inflammation within the gastrointestinal tract by suppressing neutrophil activity and nuclear factor κB–dependent proinflammatory gene expression in colonocytes (*40*–*42*). Similarly, trichostatin A (TSA) is an organic compound that functions as a potent inhibitor of class I/II HDACs and has been shown to bind human SIRT-6 that can suppress cellular inflammatory responses and promote neutrophil apoptosis (*43*–*46*). Because of these results, HDACs and sirtuins are emerging therapeutic targets for the development of treatments for various inflammatory disorders, including those of the gastrointestinal tract.

In the present study, we initially sought to identify nucleases in *C. jejuni* that promote the evasion of NETs during infection by screening a transposon library for mutants that are unable to degrade neutrophil DNA. From this screen, we identified that a transposon insertion in a locus (Cjj81176_0779) that we determined was unable to degrade DNA due to polar effects on a downstream nuclease but that we subsequently found was unable to activate and induce NET production by human neutrophils. Computational analysis of the protein predicted to be encoded by Cjj81176_0779 revealed secondary structure homology to various bacterial and eukaryotic sirtuins. In-frame deletion mutants of this determinant, which we call SliP for sirtuin-like protein, were reproducibly reduced for activation and NET production by human neutrophils, and activation could be complemented by expressing *sliP* in trans. We further found that purified SliP deacetylates acetyl-lysine peptides in a nicotinamide adenine dinucleotide (oxidized form) (NAD^+)–dependent manner and that zinc augments this activity, which is consistent with the prediction that SliP functions as a sirtuin. Furthermore, we found that SliP can be translocated from the bacterium in a flagella-dependent manner, including within human neutrophils. Following secretion, SliP could then associate with neutrophil histones, which correlated with reduced acetylation of these structures. Last, we demonstrate that inflammation and intestinal pathology are promoted by SliP despite the mutant being able to efficiently colonize the host gastrointestinal tract. These findings suggest that histone deacetylation mediated by SliP is a previously unidentified mechanism by which a pathogen induces an inflammatory response and tissue pathology during infection. With these findings, we expect that therapeutic strategies can be developed to mitigate SliP-dependent inflammation and pathology during acute and chronic human campylobacteriosis.

Table 1. Transposon insertion mutants that exhibited a significant reduction in DNA degrading activity within cell-free supernatants.

Locus	Predicted gene function (predicted gene name)
CJJ81176_0025	Flagellar hook protein (*flgE*)
CJJ81176_0252	Acetylornithine aminotransferase (*argD*)
CJJ81176_0580	Membrane protein (*citT*)
CJJ81176_0644	Phosphate ABC transporter, permease protein (*pstA*)
CJJ81176_0779	DUF4917 family protein
CJJ81176_0803	Ferredoxin-type protein (*napH*)
CJJ81176_0936	Cytosol aminopeptidase
CJJ81176_1243	Chaperone protein (*dnaJ-1*)
CJJ81176_1270	DNA glycohydrolase (*mugA*)
CJJ81176_1353	Enterochelin ABC transporter, ATP-binding protein (*ceuD*)
CJJ81176_1425	HrEpiB
CJJ81176_1585	Histidinol dehydrogenase (*hisD*)

RESULTS

C. jejuni has several genes that promote neutrophil DNA degradation and may be involved in NET evasion

Because we have established that *C. jejuni* induces NET production and that NETs do not substantially affect the viability of the bacterium during coincubation, we hypothesized that *C. jejuni* maintains an array of genes that facilitate the degradation of NETs as an evasion strategy. To identify these determinants, we used a previously established *C. jejuni* transposon mutant library (*61*) to screen 8640 individual mutants for extracellular nuclease activity on a commercially available deoxyribonuclease (DNase) agar. From this primary screen, we identified 130 isolates that lacked a zone of clearing around the colony, which was indicative of an extracellular nuclease–deficient phenotype (Fig. 1A). To confirm and quantify this phenotype, we conducted a secondary screen using deoxycholate (DOC)–induced, cell-free supernatants from these strains where we incubated these supernatants with neutrophil genomic DNA and used quantitative polymerase chain reaction (qPCR) quantify the amount of intact *Homo sapiens GAPDH*. After this secondary screen, 12 transposon mutant reproducibility exhibited a reduction in the ability of their cell-free supernatants to significantly decrease ($P < 0.05$) the amount of intact neutrophil DNA (Table 1), including an insertion into Cjj81176_0779 (Fig. 1B). Before examining NET evasion by nuclease-deficient

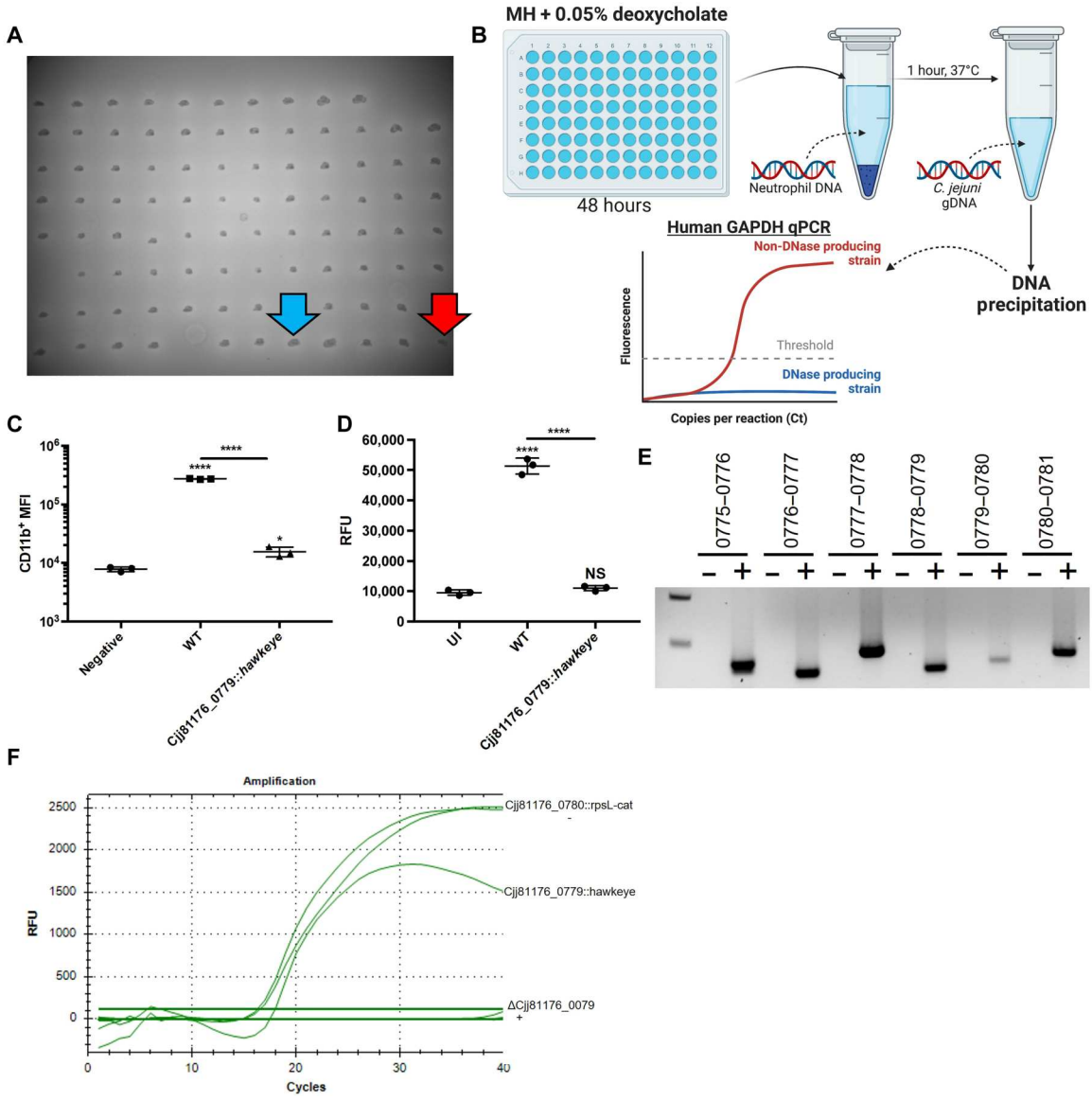

Fig. 1. Transposon mutagenesis screen identifies *C. jejuni* operon necessary for nuclease production and neutrophil activation. (**A**) Primary nuclease screen where individual transposon isolates were stamped on DNase agar for 2-day growth. Nuclease production was indicated by the presence of clearance around the colonies (blue arrow), whereby some colonies lacked zones of clearance (red arrow). (**B**) Secondary qPCR screen identified transposon isolates lacking a cell-free supernatant–associated nuclease. Supernatants were incubated with neutrophil DNA for 1 hour, and then *C. jejuni* genomic DNA (gDNA) was spiked in afterward as a DNA precipitation extraction control. Neutrophil and *C. jejuni* DNA were quantified through qPCR. (**C**) A transposon mutant isolate in Cjj81176_0779 had reduced neutrophil activation and (**D**) NETosis. (**E**) Cjj81176_0779 is encoded within an operon with a predicted nuclease, Cjj81176_0780. Operonic PCRs of intergenic regions were performed from cDNA of RNA extracted from *C. jejuni* incubated with neutrophils. Reverse-transcribed RNA (+) and nonreverse-transcribed RNA (−) were analyzed through standard PCR and resolved on an agarose gel for imaging. (**F**) Amplification plots of DNA incubated with mutants of Cjj81176_0779 and Cjj81176_0780 demonstrate polar effects of Cjj81176_0779 transposon insertion. DNA was also incubated with medium alone (−) and pure DNase (+) to serve as negative and positive controls, respectively. The data are representative of biological triplicate. Multiple comparison testing was performed using analysis of variance (ANOVA) with Tukey's post hoc test. *$P < 0.05$; ****$P < 0.0001$. MFI, mean fluorescence intensity; WT, wild-type; RFU, relative fluorescence units; NS, not significant; UI, uninfected.

mutants of *C. jejuni*, we first wanted to establish whether human neutrophils were activated and produced NETs in response to these mutants. Using the transposon mutant of CJJ81176_0779, we infected primary human neutrophils and examined for activation of cells within the population using CD11b, finding that the mutant-infected neutrophils exhibited a 17.36-fold decrease in $CD11b^+$ cells compared to wild-type–infected neutrophils and a 2.00-fold increase compared to uninfected neutrophils (Fig. 1C). In addition, when NET induction was analyzed through SYTOX staining, NET staining was significantly decreased, with a 4.67-fold decrease compared to wild-type–infected neutrophils and 1.15-fold increase compared to uninfected neutrophils with no significant up-regulation of apoptosis (Fig. 1D and fig. S1).

Cjj81176_0779 is in an operon (Fig. 1E) that contains a gene predicted to encode the R chain of a type I site-specific DNase (Cjj81176_0780) so we sought to determine whether polar effects on Cjj81176_0780 may explain the nuclease-deficient phenotype of the Cjj81176_0779 transposon mutant. To accomplish this, we constructed an in-frame deletion mutant of Cjj81176_0779 and an insertion-deletion mutant of Cjj81176_0780 and examined nuclease activity using the above qPCR assay on cell-free supernatants. We found that the Cjj81176_0779 deletion mutant retained nuclease activity and that the integrity of neutrophil DNA was maintained during incubation with Cjj81176_0780 mutant supernatants, which strongly suggests that our initial transposon mutant result that Cjj81176_0779 promotes DNA degradation was due to a polar effect on Cjj81176_0780 (Fig. 1F). Furthermore, we determined that reduced neutrophil activation and NET production were associated with Cjj81176_0779 and not Cjj81176_0780 (below), which is why we focused on the characterization of the Cjj81176_0779 gene product.

Cjj81176_0779 was predicted to encode a sirtuin-like deacetylase that is more frequently present in clinical isolates than agricultural or environmental isolates

BLAST analysis of Cjj81176_0779 found the predicted protein contains a DUF4917 domain that shares homology with other pathogen-derived DUF4917 family proteins, including those from *Yersinia enterocolitica* and *Legionella pneumophila* (Fig. 2A) (*47*, *48*). Despite DUF4917 proteins being present in the above microorganisms, as well as many other representatives in *Burkholderia* and *Brucella* species, little is known about the function of these proteins [European Molecular Biology Laboratory-European Bioinformatics Institute (EMBL-EBI)]. Beyond determining that Cjj81176_0779 is a member of the DUF4917 family, we also determined it is downstream of *dnaK* and *grpE*, both of which are chaperones involved in flagellar biogenesis and chaperoning type III secretion system (T3SS) effectors in other organisms (Fig. 2B) (*49*, *50*). As the DUF4917 family of proteins has yet to be investigated for function, secondary structure prediction was performed using Phyre2 and Iterative Threading ASSEmbly Refinement (I-TASSER) (*51*, *52*). In both analyses, the protein encoded by Cjj81176_0779 shares predicted secondary structure homology to various bacterial sirtuins and human SIRT2; hence, this protein was named and is hereafter referred to as SliP (Fig. 2B). Important to these analyses, SliP appears to contain a Rossman fold, which is present in many sirtuins as a G-X-G motif that is responsible for binding the phosphate group of NAD^+ along with a small pocket of charged amino acids that bind the two ribose molecules of NAD^+ (Fig. 2, C and D) (*53*). The predicted Rossman fold in SliP exists as a G-N-G motif, and the second glycine residue at position 26 (G26) was predicted to bind NAD^+ by iTASSER (Fig. 2E and movie S1). To determine the potential role of this protein in the pathogenesis of *C. jejuni*, we examined for *sliP* in the genomes of agricultural and environmental isolates of *C. jejuni* and compared that incidence to human clinical

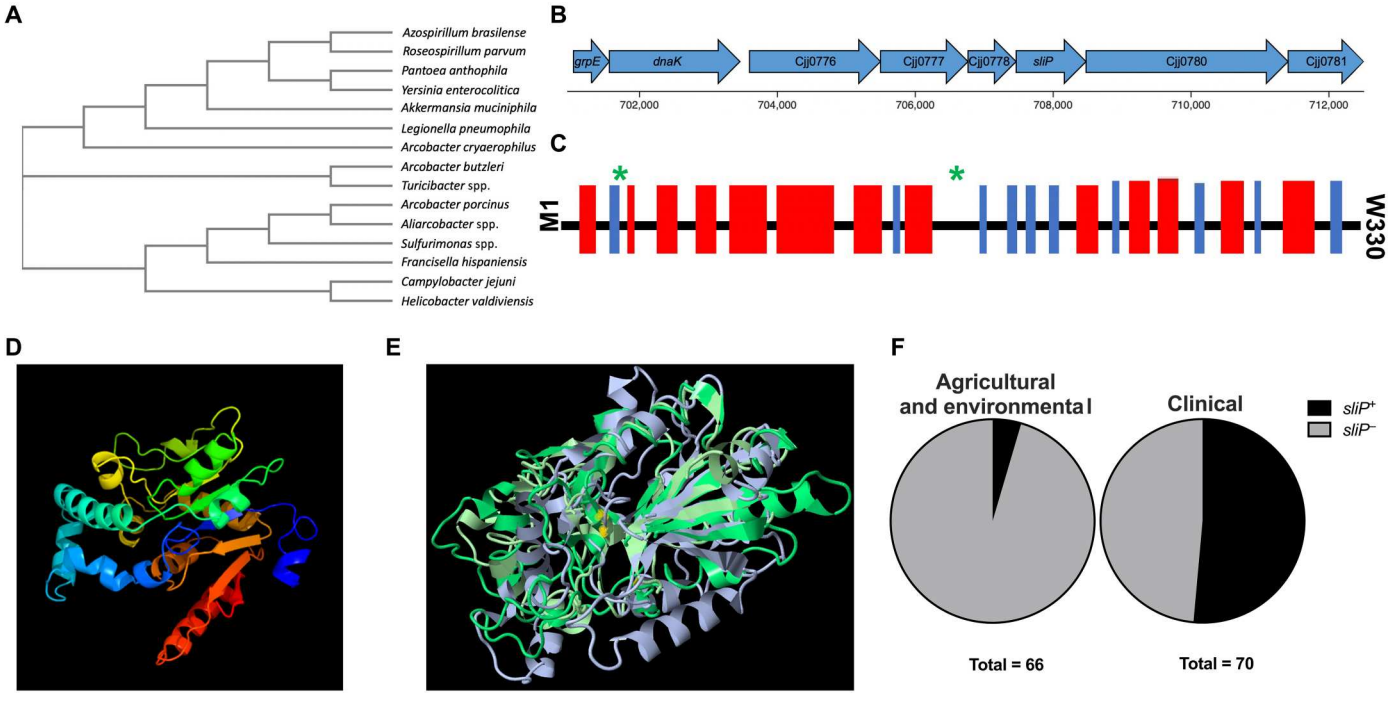

Fig. 2. Identification of the predicted sirtuin, SliP, in *C. jejuni*. (**A**) Phylogenetic analysis of the DUF4917 family proteins in relation to *C. jejuni*. A BLAST analysis was performed for proteins homologous to the *C. jejuni* DUF4917 family protein. (**B**) Gene neighborhood of *sliP* within the *C. jejuni* genome. Predicted operons were done through Microbial Signal Transduction Database analysis. (**C**) Predicted protein scheme of SliP secondary structure through iTASSER analysis. Black bars designate coils, blue bars represent strands, and red bars represent helices. Green asterisks designate predicted Rossman fold domains within SliP. (**D**) Prediction of the secondary structure of SliP using Phyre2 threaded through the *Bacillus subtilis* ThsA, the highest amino acid similarity protein to SliP. (**E**) Overlapped secondary structure models of DUF4917 family proteins using Jmol software. Yellow dots indicate position of the G26 residue within the structural model for the representative *C. jejuni* SliP shown. (**F**) Percentage of *sliP* containing environmental and clinical *C. jejuni* genomes from a previous study. Whole genomes were uploaded to KBase, where the homology threshold was set to 75%. Chi-square contingency testing was performed, $\chi^2 = 36.51$, $z = 6.042$, $P \leq 0.0001$.

isolates collected and sequenced in a previous study (*54*). We found that *sliP* is more frequently present in clinical isolates, with 36 of 70 isolates encoding *sliP* (Fig. 2F) and only 3 of 66 agricultural and environmental *C. jejuni* having the gene ($\chi = 36.51$, $z = 6.042$, $P \leq 0.0001$).

SliP functions as a canonical sirtuin by deacetylating lysines using NAD$^+$ and zinc cofactor

To investigate the function of SliP, we purified His-tagged protein by Ni–nitrilotriacetic acid (NTA) chromatography (fig. S2, A, B, and F). Because NAD$^+$ and zinc are often required for sirtuin activity (*55*), the deacetylase activity of purified SliP was determined for acetyl-lysine peptides with or without those cofactors. As expected, when either 5 mM NAD$^+$ or 20 μM zinc chloride was individually added to deacetylase reactions, there were 1.92- and 3.11-fold increases in lysine deacetylation after 1 hour when compared to reactions without the cofactors, respectively. When both NAD$^+$ and zinc chloride were added, we observed a 3.76-fold increase in lysine deacetylation when compared to reactions without the cofactors (Fig. 3A). As sirtuins classically hydrolyze NAD$^+$ during lysine deacetylation (*56*), we sought to determine whether SliP-mediated deacetylation leads to NAD$^+$ hydrolysis. Using purified SliP, NAD$^+$ concentrations were monitored over time during lysine deacetylation using a commercially available kit, with purified human SIRT2 used as a positive control and a mock purification from an *Escherichia coli* background (empty vector) as a negative control, for both NAD$^+$ hydrolysis and lysine deacetylation. As expected, NAD$^+$ concentrations decreased 1.94- and 2.06-fold during deacetylation of acetyl-lysine peptides by purified N- and C-terminal His-tagged SliP, respectively, while the negative controls were unable to significantly decrease NAD$^+$ concentrations (1.07- and 1.06-fold reductions for N- and C-terminal His-tagged vectors, respectively) (Fig. 3B and fig. S2, G and H). Deacetylase reactions containing SliP or the negative control eluates did not result in significant hydrolysis of reduced form of NAD$^+$ (NADH) (fig. S3). To determine whether the conserved glycine residues in SliP (Fig. 1, C and E) are required for sirtuin activity, we introduced individual single point mutations into SliP (SliP$_{G24A}$ and SliP$_{G26A}$) along with a double amino point mutation (SliP$_{G24A,G26A}$) (fig. S2, C to E). Compared to wild-type SliP, SliP$_{G24A}$ and SliP$_{G26A}$ were less able to hydrolyze NAD$^+$ as readily, exhibiting 1.58- and 1.42-fold increases in NAD$^+$ concentration, respectively (Fig. 3B). Accordingly, compared to wild-type SliP, SliP$_{G24A}$ and SliP$_{G26A}$ performed less lysine deacetylation, having 1.74- and 1.92-fold decreases in deacetylated lysine residues (Fig. 3C). However, when both glycine residues are mutated to alanines, there were significant 1.86-fold increase in NAD$^+$ concentration and 5.31-fold decrease in lysine deacetylation compared to wild-type SliP–incubated reactions (Fig. 3, B and C). By comparison, SIRT2 was able to efficiently deacetylate lysines and hydrolyze NAD$^+$ in vitro, with an observed 12.18-fold increase in lysine deacetylation and 3.00-fold decrease in NAD$^+$ concentrations (Fig. 3, B and C). On the basis of these results, we concluded that SliP functions as a canonical sirtuin, that the glycine residues within the predicted Rossman fold participate in NAD$^+$ binding and hydrolysis during lysine deacetylation, and that more work needs to be conducted to define the ideal conditions for SliP activity in vitro.

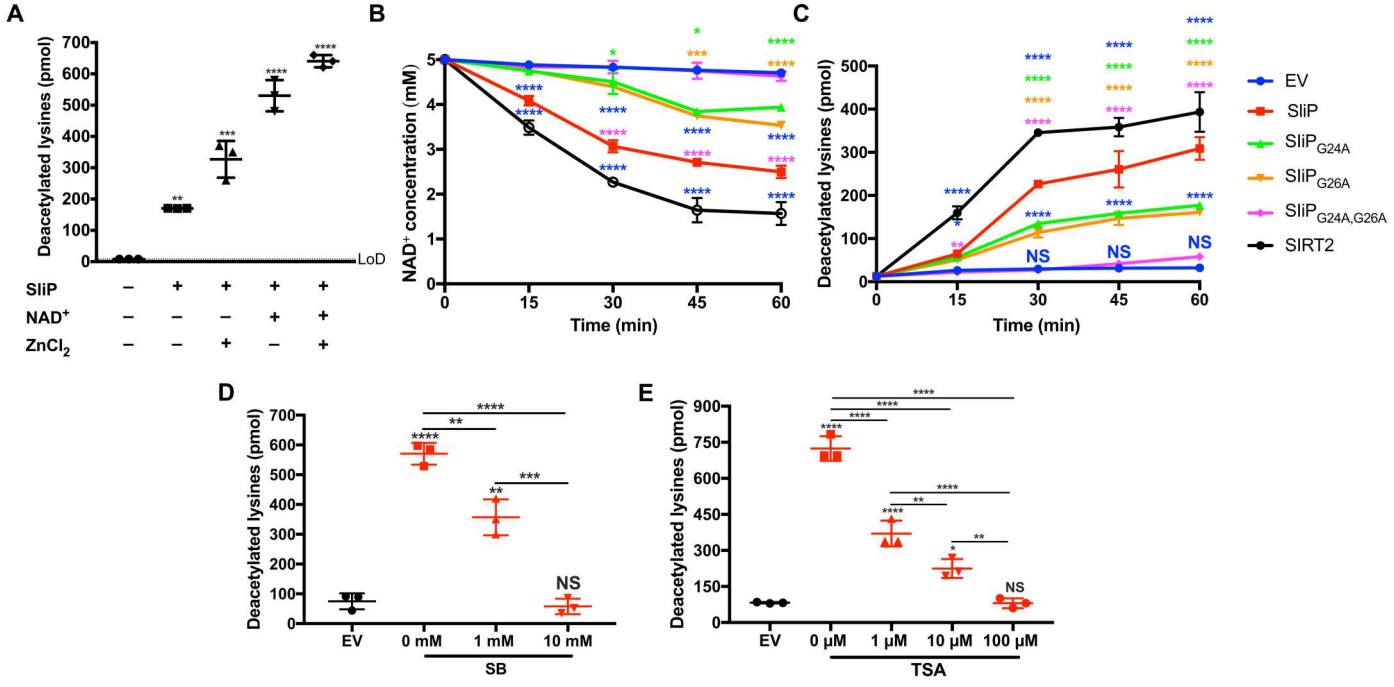

Fig. 3. SliP is an NAD$^+$-dependent sirtuin and requires zinc for maximal activity. (**A**) Lysine deacetylation was performed for SliP with common sirtuin cofactors, NAD$^+$ and zinc chloride, and assayed after 1 hour after incubation at 37°C. For statistical analysis, each treatment group was compared to the empty vector (EV) control. (**B**) NAD$^+$ hydrolysis assay and (**C**) lysine deacetylation during a 1-hour time course at 37°C. Blue bars represent the EV controls, SliP is represented in red, SliP$_{G24A}$ reactions are depicted in green, SliP$_{G26A}$-incubated reactions are represented in orange, and SliP$_{G24A,G26A}$ reactions are depicted in pink. Pure SIRT2 is represented in black lines. (**D**) Sodium butyrate (SB) and (**E**) TSA dose-response analysis of SliP inhibition after 1 hour after incubation at 37°C. Multiple comparison testing was performed using ANOVA with Tukey's post hoc test. *$P < 0.05$; **$P < 0.01$; ***$P < 0.001$; ****$P < 0.0001$.

To further define SliP's role as a sirtuin, we sought to determine whether characterized deacetylase inhibitors can reduce SliP activity. To accomplish this, we used conditions where maximum lysine deacetylation was observed in vitro and titrated in medium alone, sodium butyrate (SB), or TSA and assayed for lysine deacetylation as above. We observed a dose-dependent inhibition of deacetylation for both SB and TSA to where at 10 mM (for SB) and 100 μM (for TSA), the presence of SliP did not lead to significantly more deacetylation than when eluates lacking a deacetylase were used. For example, there were a 9.85-fold reduction in lysine deacetylation at 10 mM SB (Fig. 3D) and a 9.01-fold reduction in lysine deacetylation at 100 μM TSA (Fig. 3E). These results demonstrate that SB and TSA can chemically inhibit SliP-dependent lysine deacetylation, which supports the conclusion that SliP functions as a sirtuin having deacetylase activity.

SliP is required for neutrophil activation and NET production by *C. jejuni* through its deacetylase activity

On the basis of the reduced neutrophil activation and NETosis that was observed for the *sliP* transposon mutant, we sought to determine whether this result was due exclusively to interruption of *sliP* or whether it was due to polar effects—similar to our DNA degradation data. To address this, we constructed an in-frame deletion mutant of *sliP* (Δ*sliP*), as well as a complemented version of this strain expressing *sliP* in trans, and compared their ability to activate neutrophils to that of wild-type *C. jejuni* and an insertion-deletion mutant of Cjj81176_0780 (Cjj81176_0780::*rpsL-cat*) during infection of primary human neutrophils. Using CD11b as an output of neutrophil activation, infection with wild-type *C. jejuni* resulted in 22.37-fold more $CD11b^+$ neutrophils when compared to uninfected controls, while Δ*sliP*-infected neutrophils exhibited only a 2.53-fold increase in the $CD11b^+$ population (Fig. 4A). This represents a significant reduction in neutrophil activation when compared to wild-type–infected cells. Further, when we infected human neutrophils with Δ*sliP*-complemented in trans, a 24.55-fold increase in the number of $CD11b^+$ neutrophils was observed when compared to uninfected controls (Fig. 4A). In contrast, when neutrophils were infected with Cjj81176_0780::*rpsL-cat*, neutrophil activation was maintained at levels similar to wild-type–infected neutrophils, with a 22.49-fold increase in the $CD11b^+$ population relative to uninfected neutrophils (Fig. 4A).

When NET production was evaluated, infection with wild-type *C. jejuni* led to a 4.17-fold increase in extracellular DNA when compared to uninfected neutrophils using fluorescent staining (Fig. 4B) (*7*). Similar to the activation results from above, Δ*sliP*-infected neutrophils exhibited only a 1.10-fold increase in extracellular DNA when compared to uninfected neutrophils, which represents a significant decrease from what was observed using wild-type *C. jejuni* (Fig. 4B). When the complemented Δ*sliP* mutant was used, extracellular DNA increased 4.07-fold relative to uninfected cells (Fig. 4B). Furthermore, a 4.26-fold increase in extracellular DNA was observed when neutrophils were infected with the Cjj81176_0780::*rpsL-cat* (Fig. 4B). The above results strongly suggest that *sliP* is involved in neutrophil activation and resulting NETosis independent of Cjj81176_0780. Because of the importance of these observations, we examined for *sliP*-dependent accumulation of PAD4 in *C. jejuni*–infected neutrophils and obtained fold changes relative to uninfected neutrophils of 12.95, 1.03, and 12.23 for wild-type, Δ*sliP*, and complemented Δ*sliP*, respectively (Fig. 4C). The compelling results from the experiments above indicate that *sliP* is specifically required for the activation of neutrophils and the associated production of NETs. Because both innate immune responses have been predicted to be required for disease during campylobacteriosis, the identification of SliP provided us with an opportunity to both better understand how *C. jejuni* induces neutrophil activation and whether neutrophil actions are responsible for gastrointestinal disease.

To determine whether neutrophil activation and extracellular trap formation were associated with the deacetylase activity of SliP, we also compared activation of a Δ*sliP* strain complemented with $sliP_{G24A}$, $sliP_{G26A}$, or $sliP_{G24A,G26A}$ to uninfected, wild-type–infected, and mutant-infected neutrophils. This infection resulted in 1.30- and 1.53-fold decreases in $CD11b^+$ cell abundance in $sliP_{G24A}$ and $sliP_{G26A}$ complement–infected neutrophils compared to the wild-type *sliP* complement strain–infected neutrophils (Fig. 4D). However, $sliP_{G24A,G26A}$ complement–infected neutrophils displayed a significant 4.93-fold decrease in $CD11b^+$ cell abundance compared to wild-type *sliP* complement–infected neutrophils (1.49-fold increase compared to *sliP* mutant–infected neutrophils) (Fig. 4D). Furthermore, when NET production was evaluated using fluorescent staining of extracellular DNA (*7*), similar to our activation results, $sliP_{G24A}$ and $sliP_{G26A}$ variant–infected neutrophils exhibited intermediate 2.50- and 2.40-fold increases in extracellular DNA when compared to uninfected neutrophils (Fig. 4E). However, double substitution $sliP_{G24A,G26A}$ variant–infected neutrophils exhibited only a 1.63-fold increase in extracellular DNA when compared to uninfected neutrophils (Fig. 4E). Hence, the Rossman fold within SliP is crucial not only for the deacetylase activity of the protein but also for the activation and subsequent NETosis of human neutrophils. To determine whether other bacterial deacetylases may be involved in neutrophil activation and NETosis, we examined the above phenotypes in a transposon mutant of the predicted intracellular sirtuin, *cobB*. In contrast to Δ*sliP* responses, all neutrophil activities elicited by *cobB*::*hawkeye* resembled those of wild-type–infected neutrophils (fig. S4). As a result, we concluded that SliP plays a crucial role in modulating neutrophil responses to *C. jejuni,* perhaps through its deacetylation of host proteins, independent of any other known bacterial sirtuin.

To determine whether chemical inhibition of SliP deacetylase activity reduces neutrophil activation and NETosis, we preincubated neutrophils with SB and TSA at the concentrations that inhibited SliP-dependent deacetylation from above. When neutrophils were preincubated with these inhibitors and then infected with wild-type *C. jejuni*, we observed significant 1.2- and 2.0-fold reductions in $CD11b^+$ neutrophil populations when SB and TSA were added, respectively (Fig. 4F). This reduced activation also resulted in a significant decrease in NETosis, with SB and TSA treatments leading to 1.71- and a 2.30-fold reductions in extracellular DNA, respectively (Fig. 4G). Supporting this result, PAD4 levels were also significantly reduced in SB- and TSA-treated neutrophils during infection with wild-type *C. jejuni* (fig. S5). These results further support that SliP may promote neutrophil activation and NET induction through deacetylation of host proteins and that treating infections with known deacetylase inhibitors may be possible.

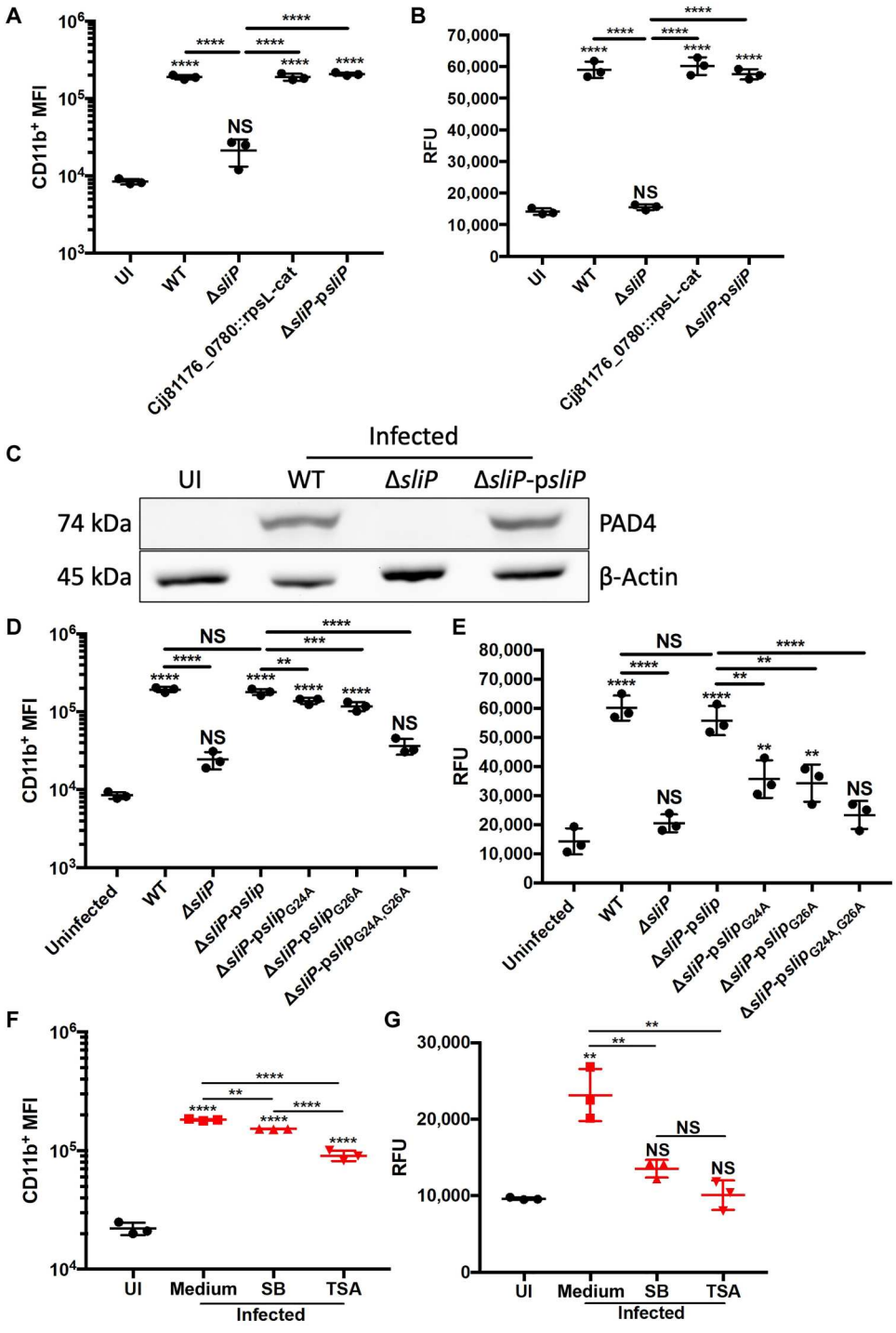

Fig. 4. SliP is necessary for *C. jejuni*–induced neutrophil activation and NETosis. (**A**) SliP is responsible for *C. jejuni*–induced neutrophil activation through flow cytometry analysis of CD11b expression. (**B**) *C. jejuni*–induced NETs are dependent on SliP presence within the bacterium. NETs were quantified through an extracellular DNA SYTOX assay. (**C**) PAD4 expression in neutrophils infected with *C. jejuni* expressing SliP for 3 hours under microaerobic conditions. (**D**) Sirtuin activity of SliP promotes neutrophil activation through flow cytometry analysis of CD11b expression. (**E**) Sirtuin activity of SliP leads to induction of NETs through an extracellular DNA SYTOX assay. (**F**) Inhibition of SliP-dependent neutrophil activation and (**G**) NET generation using SB and TSA. The data are representative of biological triplicate. Multiple comparison testing was performed using ANOVA with Tukey's post hoc test. $^{**}P < 0.01$; $^{***}P < 0.001$; $^{****}P < 0.0001$.

Functional SliP is translocated from *C. jejuni* in a manner that requires the flagella and a DOC signal

Because neutrophils were reduced for activation and NET production in response to a *sliP* mutant, we hypothesized that SliP may be translocated from the bacterium into the host. To initially examine this, we first established whether SliP can be secreted from *C. jejuni* by raising polyclonal antibodies against purified His-tagged *C. jejuni* SliP and assaying cell-free supernatants for the presence of the protein by Western blot. In addition, because DOC has been shown to promote secretion by *C. jejuni* through the flagellar secretion system (*57*, *58*), we investigated whether SliP translocation into culture supernatants increased in response to sodium DOC and whether SliP secretion was absent in a nonflagellar mutant of *C. jejuni* (Δ*flgE*). Regardless of whether strains were grown with or without DOC, SliP was detected in whole-cell lysates of each strain except for Δ*sliP* (Fig. 5A). When we examined for translocation of SliP into medium lacking sodium DOC, we did not detect SliP in cell-free supernatants. In contrast, when strains were grown in medium containing sodium DOC, SliP was detected in cell-free supernatants of all strains except the Δ*sliP* and Δ*flgE* mutants (Fig. 5A). Furthermore, when we probed for a known intracellular protein, RNA polymerase subunit alpha (RpoA), we only observed protein within cell pellets and not within supernatant regardless of medium condition, which indicates that the presence of SliP was not due to cell lysis (Fig. 5A) (*59*). To further confirm this, we quantified the amount of *C. jejuni* genomic DNA in supernatants with or without sodium DOC by qPCR and observed no significant differences across strains or growth conditions. By comparison, genomic DNA was readily amplified once cells were incubated in the presence of SDS (fig. S6). The above results support the conclusion that SliP can be translocated through the flagellar secretion apparatus in response to an intestinal signal similar to DOC.

To determine whether translocated SliP is functional, we investigated cell-free supernatants of cultures grown in medium supplemented with sodium DOC for sirtuin activities, including NAD^+ hydrolysis and lysine deacetylation. We observed significant

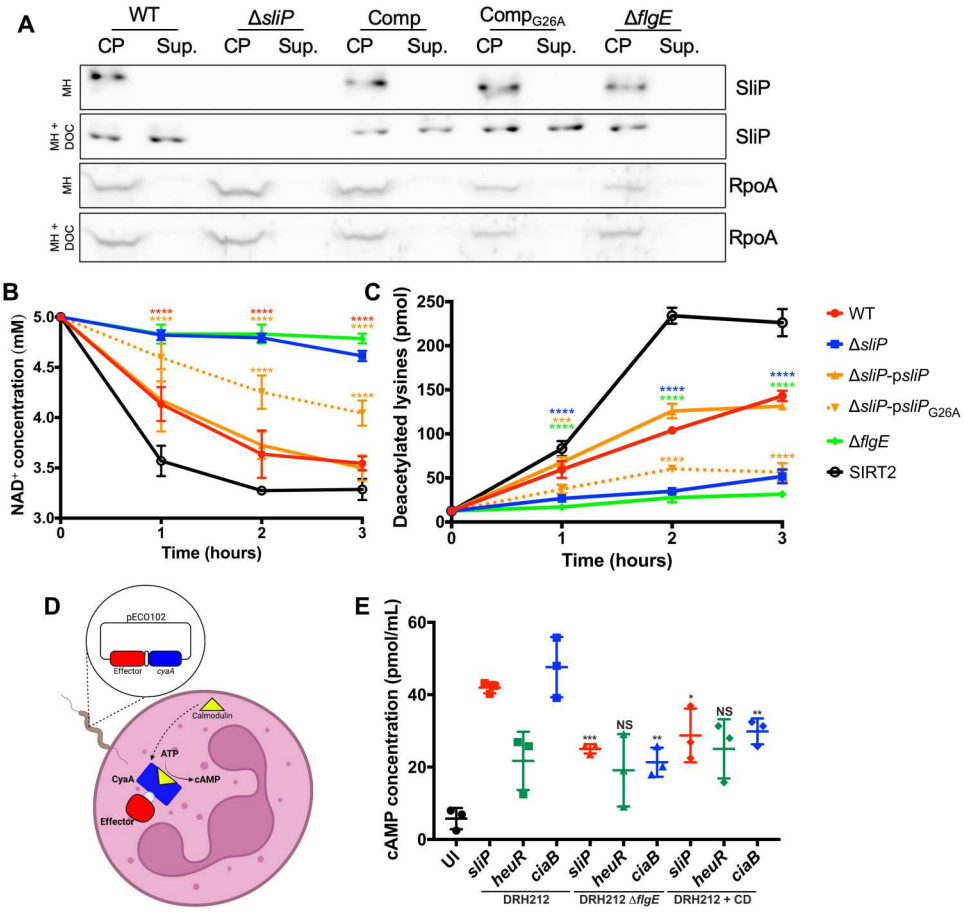

Fig. 5. SliP is translocated into host neutrophils through the flagellar secretion system. (**A**) DOC induces SliP translocation through the flagella into the supernatant. Cultures were grown in Mueller-Hinton (MH) broth alone (MH) or supplemented with DOC (MH + DOC) for 48 hours under microaerobic conditions. Whole-cell lysates (CP) and supernatants (sup.) were analyzed for SliP abundance by Western blot. Cell pellets and supernatants were also analyzed for RpoA, serving as a negative control. (**B**) NAD^+ hydrolysis during (**C**) lysine deacetylation using supernatants over a 1-hour incubation period at 37°C. Pure SIRT2 was used as a positive control for both NAD^+ hydrolysis and lysine deacetylation (black lines). (**D**) Schematic for the calmodulin-dependent *B. pertussis* adenylate cyclase (CyaA) bacterial secretion assay for *C. jejuni* within neutrophils. (**E**) CyaA translocation assay performed in wild-type– and the flagella mutant (Δ*flgE*)–infected neutrophils. The *ciaB-cyaA* and *heuR-cyaA* translational fusions served as positive and negative controls, respectively. The data are representative of biological triplicate. Multiple comparison testing was performed using ANOVA with Tukey's post hoc test. *$P < 0.05$; **$P < 0.01$; ***$P < 0.001$; ****$P < 0.0001$. ATP, adenosine 5′-triphosphate.

NAD^+ hydrolysis in supernatants from both wild-type and *sliP*-complemented strains, with 1.41- and 1.42-fold respective decreases in NAD^+ concentrations when compared to the starting concentration. In addition, the complemented strain harboring the G26A mutation exhibited a 1.16-fold increase in NAD^+ concentrations relative to the Δ*sliP* complemented with wild-type *sliP*. In contrast, supernatants from both Δ*sliP* and a flagellar hook mutant (Δ*flgE*) did not produce significant NAD^+ hydrolysis following 1-hour incubation with only 1.08- and 1.04-fold decreases relative to the starting concentrations of NAD^+ (Fig. 5B). When we examined for deacetylase activity within the supernatants of wild-type and *sliP*-complemented strains, the number of lysines deacetylated was increased by 11.45- and 10.52-fold when compared to the 0-hour time point, respectively. As expected, supernatants from the Δ*sliP* and Δ*flgE* mutants were unable to significantly deacetylate lysine residues, exhibiting 4.14- and 2.52-fold decreases when compared to wild-type supernatants, respectively. Last, Δ*sliP* complemented with the G26A variant exhibited a 2.32-fold decrease in deacetylated lysines when compared to Δ*sliP* complemented with wild-type *sliP* (Fig. 5, B and C). For the SIRT2-positive control, there was an 18.1-fold increase in lysine deacetylation compared to the 0-hour time point. In addition, there was a significant 1.52-fold decrease in NAD^+ concentrations when compared to the starting concentration. This observation not only supports our above observations that SliP is present in *C. jejuni* supernatants, but it also suggests that it is enzymatically active as a deacetylase and requires the flagellar secretion apparatus for translocation.

SliP is translocated into human neutrophils following uptake and contributes to elevated deacetylase activity in neutrophils

To investigate whether SliP is secreted into human neutrophils, we constructed a translational fusion of SliP to the *Bordetella pertussis* adenylate cyclase (CyaA) domain (Fig. 5D) (*60*). In addition to the SliP-CyaA reporter, we constructed HeuR-CyaA and CiaB-CyaA reporters as negative and positive secretion controls, respectively (*57*, *61*, *62*). Specifically, HeuR is an intracellular *C. jejuni* transcription factor predicted to not be secreted into the extracellular environment, while CiaB is a flagellar protein that has been shown to be delivered to the cytosol of host cells. These constructs were introduced into both wild-type *C. jejuni* and Δ*flgE* (*63*, *64*). Three hours after infection, adenosine 3′,5′-monophosphate (cAMP)

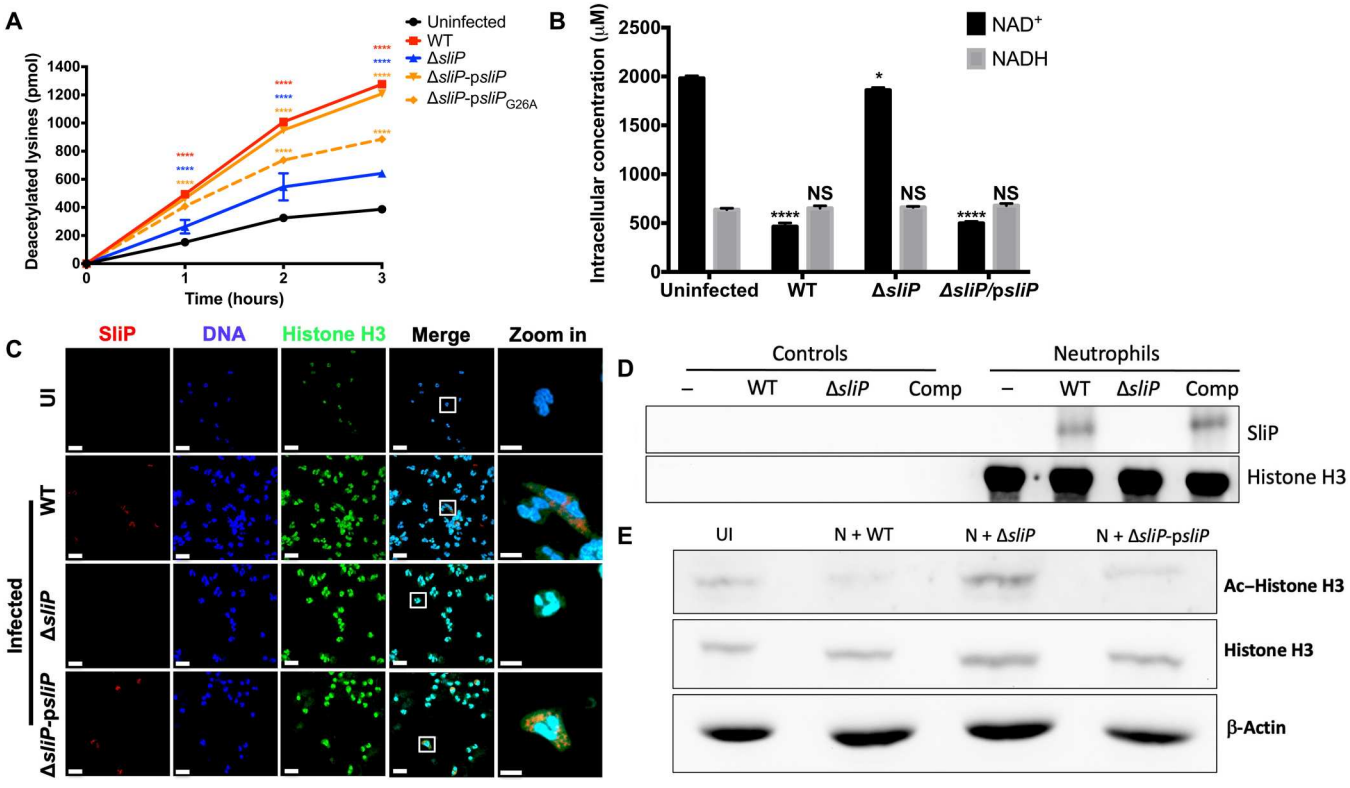

Fig. 6. *C. jejuni* neutrophil activation and NET extrusion are dependent on SliP binding and deacetylating histone H3. (**A**) Intracellular deacetylation of lysine peptides in neutrophils infected with *C. jejuni* and incubated under microaerobic conditions for up to 3 hours at 37°C. (**B**) Corresponding intracellular NAD^+ and NADH concentrations within *C. jejuni*–infected neutrophils after 3 hours at 37°C. (**C**) Colocalization of SliP with histones during neutrophil infection. Uninfected, wild-type–, Δ*sliP*–, and *sliP* complement (Δ*sliP*-p*sliP*)–infected neutrophils were stained for nuclei/DNA (blue), histone H3 (green), and SliP (red) and imaged 2 hours after infection. Scale bars, 20 μm (zoomed out images) and 5 μm (zoomed in images). Images presented are composites of three-dimensional reconstructions of z-stacked images. (**D**) Histone H3 was immunoprecipitated from *C. jejuni* wild-type–, Δ*sliP*-, and *sliP* complement–infected neutrophils. After 3 hours under microaerobic conditions, cells were fixed, and then histone H3 was pulled down using an anti–histone H3 antibody. Presence of SliP within the histone H3 complex was determined through immunoblotting. Controls included medium alone (–), wild-type bacteria alone (WT), Δ*sliP* bacteria alone (Δ*sliP*), and sliP-complemented bacteria alone (Comp). (**E**) Immunoblot of SliP-dependent neutrophil histone H3 deacetylation after bacterial infection. The data are representative of technical triplicates from a single donor. Multiple comparison testing was performed using ANOVA with Tukey's post hoc test. *$P < 0.05$; ****$P < 0.0001$

levels were measured as a proxy for effector translocation into host cells using an enzyme-linked immunosorbent assay (ELISA). In wild-type strains, cAMP levels increased by 7.26-, 3.76-, and 8.24-fold when they had the SliP-CyaA, HeuR-CyaA, and CiaB-CyaA plasmids, respectively, when compared to uninfected neutrophils. In contrast, when Δ*flgE* containing the same constructs was used to infect neutrophils, cAMP levels decreased by 1.68-, 1.13-, and 2.23-fold when compared to their wild-type SliP-CyaA, HeuR-CyaA, and CiaB-CyaA counterparts, respectively. Furthermore, wild-type strains encoding the various CyaA reporters were internalized at similar rates and produced similar amounts of adenylate cyclase despite the gene they were fused to (fig. S7, A and B); hence, any differences in cAMP concentrations were not due to differences in bacterial uptake or the expression of each fusion. Because decreased translocation of SliP into neutrophils by the Δ*flgE* mutant could be due to reduced endocytosis, we also blocked actin rearrangement using cytochalasin D (CD) to examine whether decreased uptake resulted in reduced delivery of each fusion to the neutrophil cytosol. Treatment with CD led to decreases in cAMP by 1.46-, 0.87-, and 1.6-fold when compared to untreated infection with wild-type SliP-CyaA, HeuR-CyaA, and CiaB-CyaA strains, respectively (Fig. 5E). Because actin polymerization has been implicated in *C. jejuni* invasion, neutrophil phagocytosis, and T3SS-dependent effector secretion in various organisms, further work will need to be conducted to determine how SliP is delivered to the neutrophil cytosol (*65*).

On the basis of these data, we sought to determine whether translocation of SliP results in intracellular environments that exhibit elevated lysine deacetylase activity. To accomplish this, we infected human neutrophils with wild-type *C. jejuni*, Δ*sliP*, Δ*sliP* complemented with the wild-type *sliP* (Δ*sliP*-p*sliP*), or Δ*sliP* complemented with the G26A substitution (Δ*sliP*-p$sliP_{G26A}$). As predicted, intracellular lysine deacetylation was elevated in neutrophils infected with wild-type *C. jejuni* and Δ*sliP*-p*sliP*; however, neutrophils infected with Δ*sliP* had intracellular environments that exhibited significantly reduced lysine deacetylase activity despite increased uptake of the Δ*sliP* strain into neutrophils (Fig. 6A and fig. S8). Furthermore, Δ*sliP* expressing the G26A *sliP* variant resulted in neutrophil infections where significantly less deacetylase activity was detected than when the strain had wild-type *sliP* (Fig. 6A). To support these results, we also quantified NAD^+ levels in similarly infected neutrophils. As expected, infected neutrophils having higher deacetylase activity due to the presence of wild-type SliP also exhibited significantly lower NAD^+ levels. In contrast, neutrophils infected with Δ*sliP* exhibited significantly higher levels of intracellular NAD^+ when compared to wild-type–infected neutrophils (Fig. 6B). No changes to NADH levels occurred under any condition tested (Fig. 6B). These findings support the conclusion that SliP is translocated into neutrophils and that SliP promotes deacetylase activity in neutrophils, which may result in the deacetylation of various neutrophil proteins.

SliP translocates to the cytoplasm during infection of neutrophils by *C. jejuni* and directly associates with histone H3

Following intracellular translocation, we hypothesized that a likely target of SliP-dependent deacetylation was neutrophil histones. This rationale was based on observations that histone H3 is a frequent target of posttranslational regulation and histone H3 is involved in several neutrophil behaviors, including PAD4-dependent hypercitrullination of deacetylated histone H3 before NET production (*66*). To initially examine whether this occurs, we imaged SliP during neutrophil infection using the antiserum mentioned above and examined its colocalization with histone H3 in those cells. As expected, we only detected SliP in wild-type and complemented mutant–infected neutrophils (Fig. 6C) and observed colocalization of SliP with histone H3 under these non-NETosing conditions. We observed that this colocalization was not restricted to the nucleus of infected neutrophils and was present in the cytoplasm of approximately 13% of neutrophils, potentially due to the de novo synthesis of histone H3 within the cytoplasm (Fig. 6C and fig. S9, A and B).

Because we were able to visualize SliP colocalization with histone H3 during infection, we next sought to determine whether SliP associates with histone H3 during *C. jejuni* infection of neutrophils and promotes its deacetylation. To accomplish this, we immunoprecipitated histone H3 from primary human neutrophils that were formalin-fixed following infection with wild-type *C. jejuni,* Δ*sliP*, or Δ*sliP*-p*sliP* and assayed for the presence of SliP with histone H3 complexes by immunoblot. Using this protocol, SliP was found to be present in protein complexes containing histone H3 during neutrophil infection with either wild-type *C. jejuni* or Δ*sliP*-p*sliP* (Fig. 6D). As expected, we did not detect SliP associating with histone H3 in Δ*sliP*-infected neutrophils despite purifying adequate amounts of H3 (Fig. 6D). Further, we did not detect histone H3 or SliP in either medium or bacteria-alone controls, which indicates that our anti–histone H3 antibody is specific for that protein. To eliminate nonspecific protein cross-linking as a potential explanation for SliP-H3 association, we probed for cytoplasmic lipocalin-2 (Lcn2) in those same immunoprecipitated histone H3 complexes but were unable to detect Lcn2 (fig. S10A). This suggests that SliP association with histone H3 was not due to nonspecific cross-linking of proteins to neutrophil histones. As we observed SliP association with histone H3, we next sought to investigate whether SliP affects the acetylation status of histone H3 during infection. In neutrophils infected with wild-type *C. jejuni*, histone H3 acetylation was significantly reduced by 9.57-fold when compared to the amount of histone acetylation present in uninfected neutrophils. Similar results were also observed for neutrophils infected with the complemented mutant (8.45-fold reduction compared to uninfected neutrophil levels). In contrast, Δ*sliP*-infected neutrophils displayed histone H3 acetylation intensities similar to those of uninfected neutrophils (1.12-fold reduction of uninfected result) (Fig. 6E and fig. S9C). Furthermore, when SB- and TSA-treated neutrophils were infected with wild-type *C. jejuni*, histone H3 acetylation significantly increased (fig. S5). These results support that SliP promotes neutrophil activation and NET induction through deacetylation of histone H3.

To determine whether deacetylation results may be due to the SliP-dependent recruitment of host sirtuins, we examined for the predominant human sirtuin associated with infectious diseases, SIRT2, in immunoprecipitated histone H3 complexes. Human SIRT2 was not detected in these complexes, which is a notable difference from other intracellular pathogens where these bacteria promote the recruitment of host SIRT2 to induce histone deacetylation (fig. S10A). To eliminate other host-derived factors that may posttranslationally modify histones, we examined expression of all known histone H3–targeting HDACs and HATs during infection

with *C. jejuni* and found that none of these genes were significantly affected (fig. S10B). While some HDACs and HATs appear up- and down-regulated, there were no significant differences between wild-type and Δ*sliP*-infected neutrophils, and we did not observe significant changes in SIRT2 abundance (fig. S10C). Regardless, there could be additional host HDACs performing deacetylation within the neutrophil; however, we suspect that SliP would still play a significant role. We therefore concluded that SliP translocates to the cytoplasm of infected neutrophils and directly binds to histone H3 to deacetylate the protein rather than affecting the production or localization of host-derived enzymes.

SliP promotes inflammation and gastrointestinal disease during murine campylobacteriosis

To determine whether SliP-dependent impacts on neutrophil activities affect host inflammation and gastrointestinal tissue damage during infection, we orally infected IL-10$^{-/-}$ mice with either wild-type *C. jejuni* or Δ*sliP* and examined for systemic and tissue-level impacts on the host. Before orally infecting mice, we determined that murine neutrophils behave similarly to human neutrophils when infected with *C. jejuni*, including activating similar numbers of neutrophils and inducing NETosis in those populations (fig. S11 and movie S2). When IL-10$^{-/-}$ mice were orally infected with wild-type *C. jejuni*, they exhibited significantly reduced percent weight change at days 7, 9, and 10 after infection when compared to uninfected mice (Fig. 7A). In contrast, Δ*sliP*-infected mice gained weight similar to uninfected mice, which led to significantly higher weights when compared to wild-type–infected mice at days 7 to 10 after infection (Fig. 7A). Δ*sliP* was able to colonize mice, with fecal, colonic, and cecal loads similar to wild-type–infected mice (Fig. 7, B and C, and fig. S12, A and B). In addition, we examined for bacterial dissemination from the gastrointestinal tract by determining the bacterial burden within the spleens of infected mice, finding Δ*sliP*-infected mice harbored 3.06-fold more bacteria than wild-type–infected mice (Fig. 7D). These results indicate that SliP does not affect colonization of susceptible hosts and instead suggests neutrophil activation and NET induction aids in restricting *C. jejuni* to the colon.

To determine whether SliP promotes inflammation and disease during infection, we first quantified the levels of several proinflammatory chemokines and cytokines within the serum of wild-type– and Δ*sliP*-infected IL-10$^{-/-}$ mice, including IL-1β, IL-6, interferon-γ (IFN-γ), keratinocyte-derived chemokine (KC), and TNF-α. For IL-1β concentrations, uninfected mice were observed at 83.86 ± 60.63 pg/ml, while wild-type and Δ*sliP*-infected mice were at 332 ± 138 and 122.3 ± 41.81 pg/ml, respectively (Fig. 7E). For IL-6 concentrations, uninfected mice were observed at 8.617 ± 1.535 pg/ml, while wild-type and Δ*sliP*-infected mice were at 26.33 ± 14 pg/ml and the limit of detection, respectively (Fig. 7E). Similarly, the concentration of IFN-γ in uninfected mice was determined to be 16.95 ± 13.33 pg/ml, with wild-type– and Δ*sliP*-infected mice exhibiting concentrations at 127.3 ± 70.49 and 23.92 ± 35.55 pg/ml, respectively (Fig. 7E). In uninfected mice, the concentration of KC was 13.13 ± 8.041 pg/ml, while concentrations in wild-type– and Δ*sliP*-infected mice were 40.35 ± 12.99 and 21.85 ± 12.99 pg/ml, respectively (Fig. 7E). For TNF-α, uninfected mice concentrations were observed at 19.66 ± 8.53 pg/ml, while wild-type– and Δ*sliP*-infected mice were at 53.13 ± 45.17 and 21.31 ± 9.36 pg/ml, respectively (Fig. 7E). In addition to promoting an immune response, we analyzed and scored colon pathology from wild-type– and Δ*sliP*-infected mice, including the development of edema, blood in the tissue, epithelial raggedness, and hyperplasia (*67*). When mice were infected with the Δ*sliP*, histopathological scores for the previously mentioned features were not significantly different from uninfected mice, aside from edema (Fig. 7, F and G, and fig. S12C). In support of this, we observed significant increases in neutrophil abundance (CD11b$^+$ Ly6G$^+$) within wild-type–infected mice but lowered concentrations in uninfected and Δ*sliP*-infected mice (fig. S12D). These results suggest that despite colonizing mice at levels similar to wild-type and disseminating to extraintestinal sites, the absence of SliP leaves the bacterium less immunogenic and able to cause disease in a susceptible host.

SliP associates with and promotes histone H3 deacetylation during murine infection

To connect the SliP-dependent activities that we observed in primary human neutrophils to the pathological effects that we observed in mice, we sought to demonstrate SliP association with histone H3 during infection. To initially examine this, colon sections from the above cohorts were analyzed by immunofluorescence microscopy. As expected, *C. jejuni* clusters were detected within the colons of wild-type and Δ*sliP* infected mice but not within uninfected mice (Fig. 8A). When histone H3 was examined within these clusters, increased histone acetylation colocalized in Δ*sliP*-infected mice; however, this was absent in wild-type–infected mice where histone acetylation was markedly reduced (Fig. 8A). Further, myeloperoxidase (MPO), a leukocyte-derived antimicrobial protein, was also more abundant in wild-type–infected mice than uninfected and Δ*sliP*-infected mice (Fig. 8A). To more specifically address whether SliP directly affects the acetylation status of leukocyte histones during infection, we harvested colons from uninfected, wild-type–, and Δ*sliP*-infected mice and purified CD45$^+$ immune cells. After purification, cellular proteins were cross-linked, and histone H3 was immunoprecipitated as above. After purifying histone H3 complexes, we observed SliP was present in histone H3 complexes in only wild-type–infected mice (Fig. 8, B and C). Furthermore, when the acetylation status of these complexes was examined, histone H3 acetylation was found to be reduced in wild-type–infected mice when compared to uninfected and Δ*sliP*-infected mice, both of which exhibited similar levels of acetylation (Fig. 8D). Hence, we have concluded that SliP binds to histone H3 in murine immune cells and the resulting activation of those leukocytes is in part responsible for gastrointestinal disease. In the future, we will expand on these experiments to examine for SliP-dependent impacts to the acetylome of other cell types, including colonocytes and macrophages, and whether chemical inhibition of this activity reduces disease severity.

DISCUSSION

Campylobacter species are the leading cause of bacterial-derived gastroenteritis worldwide and have broad impacts on human health that range from acute intestinal inflammation to pediatric stunting (*68*). Despite these effects, knowledge relating to how infection with *Campylobacter* species results in these outcomes is limited, but because whole-genome analyses of *C. jejuni* has suggested that the pathogen lacks many of the secretion systems and exotoxins associated with gastrointestinal pathogenesis, disease is

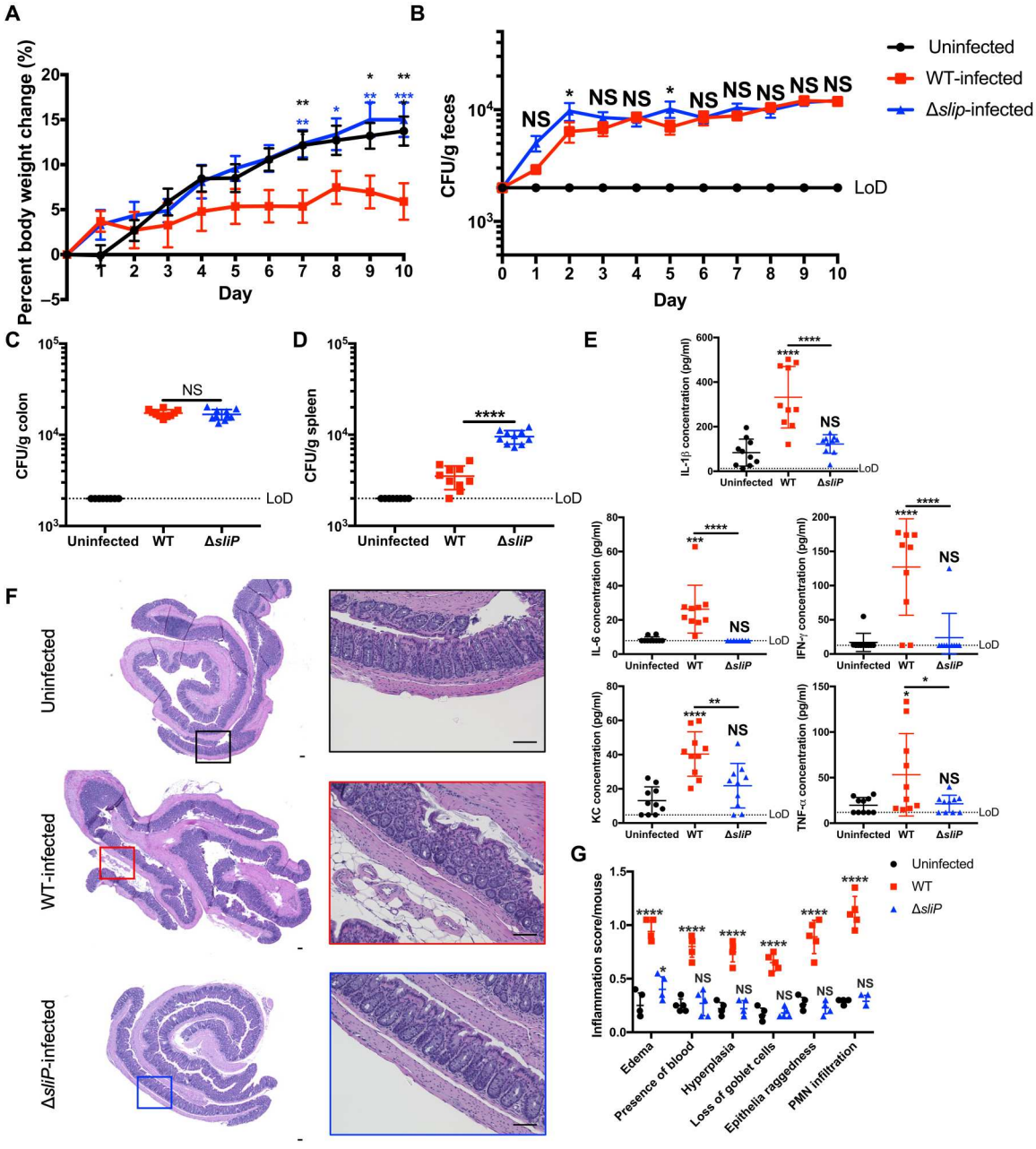

Fig. 7. SliP promotes inflammation within the IL-10$^{-/-}$ C57BL/6 mouse model of campylobacteriosis. (**A**) Percent body weight changes of mice uninfected or infected with wild-type (red) or Δ*sliP* (blue) *C. jejuni* over the 10-day infection study. Percent body weight changes were normalized to the weights of each mouse before infection. (**B**) Fecal colony-forming units (CFUs) of each cohort over the 10-day infection. Feces were collected each day and plated on *Campylobacter*-selective medium and incubated for 2 days under microaerobic conditions. (**C**) Viable CFUs from the colon and (**D**) spleen in *C. jejuni*–infected mice 10 days after infection. (**E**) Serum cytokine expression levels for each mouse per treatment group. Levels of cytokines IFN-γ, KC, IL-1β, IL-6, and TNF-α were analyzed through flow cytometry–based beads and concentrations were determined using a standard curve for each protein. Multiple comparison testing was performed using ANOVA with Tukey's post hoc test. (**F**) Hematoxylin and eosin (H&E)–stained murine colons for each representative treatment group. Scale bars, 100 μm (zoomed out and in images for each group). (**G**) Inflammation scoring from the H&E-stained colons per colon section. Analysis of inflammation scoring was performed using a nonparametric Mann-Whitney *U* test. Two rounds of mouse infections were performed on separate days, with five mice per condition each time. *$P < 0.05$; **$P < 0.01$; ***$P < 0.001$; ****$P < 0.0001$. LoD, limit of detection. PMN, polymorphonuclear neutrophil.

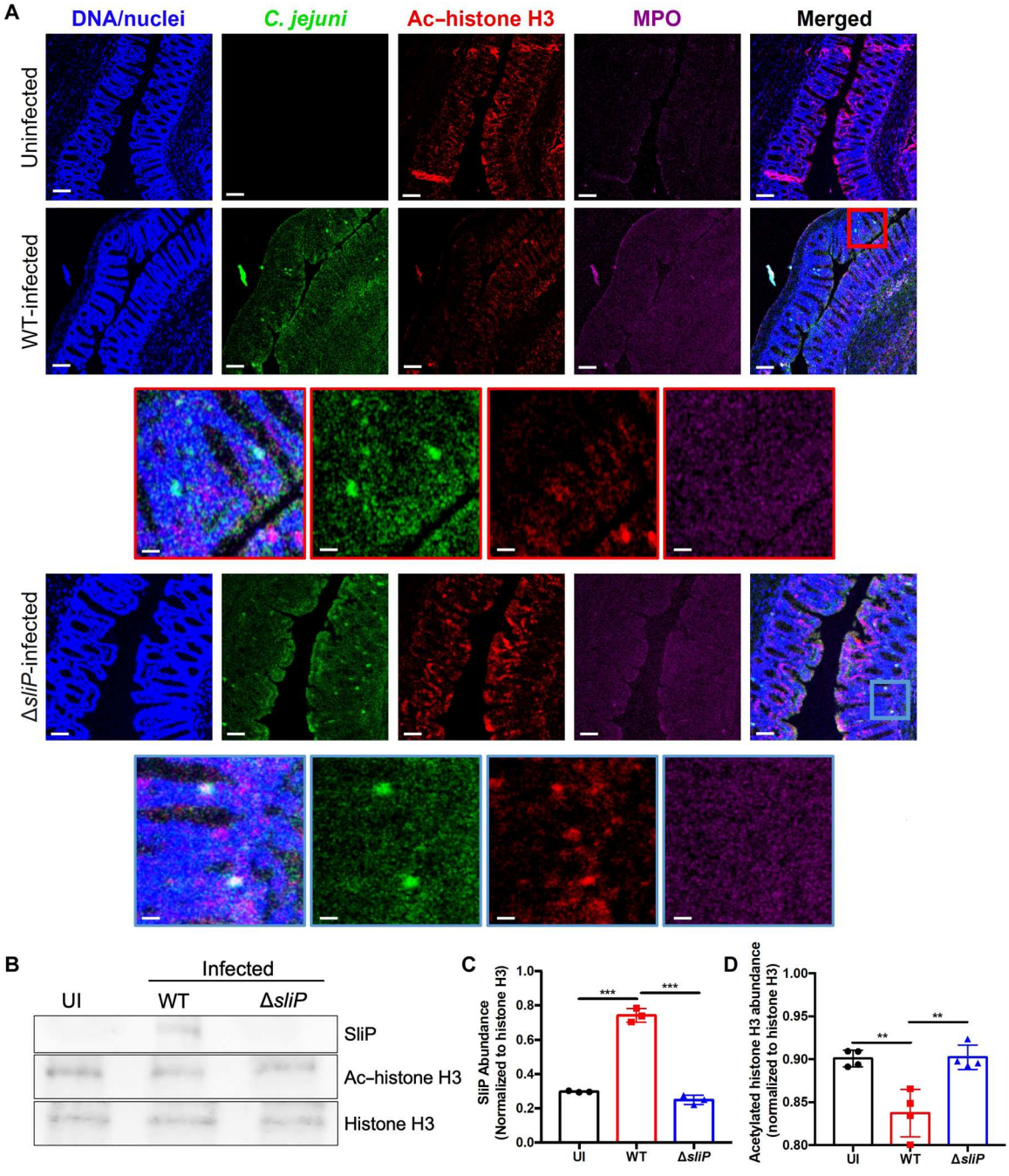

Fig. 8. In vivo detection of SliP binding to and deacetylating immune cell histone H3. (**A**) In vivo fluorescent microscopy to determine the abundance of DNA/nuclei (blue), *C. jejuni* (green), acetylated histone H3 (red), and MPO (purple) within uninfected, wild-type–, and Δ*sliP*-infected mouse colons. For each tissue section, the exposure for each channel remained constant. Images presented are individual channels and composites of z-stacked images. Scale bars, 100 μm (zoomed out images) and 10 μm [zoomed in wild-type (red border) and Δ*sliP* (blue border) images]. (**B**) Histone H3 immunoprecipitation from $CD45^+$ immune cells purified from uninfected, wild-type–, and Δ*sliP*-infected mouse colons. Presence of SliP and the acetylation of histone H3 within the histone H3 complex were determined through immunoblotting. (**C**) Densitometry analysis of SliP abundance normalized to the abundance of precipitated histone H3. (**D**) Densitometry analysis of histone H3 acetylation normalized to the abundance of precipitated histone H3. Two rounds of mouse infections were performed on separate days, with five mice per condition each time. Multiple comparison testing was performed using ANOVA with Tukey's post hoc test. *$P < 0.05$; **$P < 0.01$; ***$P < 0.001$; ****$P < 0.0001$

hypothesized to be due to dysregulated activation of the host immune response through a factor unique to *C. jejuni* (*69*). Our group previously observed that neutrophils are recruited to the colon of infected animals and that predominantly neutrophil-derived proteins are elevated in the feces of *C. jejuni*–infected patients. Because neutrophils play a key role in the development of several inflammatory diseases, some of which are related to the post-infectious disorders that occur following *C. jejuni* infection, we worked to further characterize the neutrophil response to *C. jejuni*, recently demonstrating that *C. jejuni* is a potent activator of human neutrophils and promotes the elaboration of NETs. Because several bacterial pathogens that induce NET formation have also been shown to produce nucleases that degrade those structures to facilitate evasion, we sought to identify determinants in *C. jejuni* that promote NET degradation.

Using our previously constructed transposon mutant library, we identified several insertions in *C. jejuni* that reduced nuclease production and degradation of neutrophil DNA following incubation with cell-free supernatants. One of these insertions was in a gene that is cotranscribed with the gene downstream of the insertion, which is predicted to encode for a component of a type I site-specific DNase. Experiments designed to establish the individual contributions of each of these genes found that the ability to activate and induce NET formation was associated with the gene containing the initial insertion (CJJ81176_0779), while nuclease activity was due to the downstream gene (CJJ81176_0780). Since neutrophil activities are predicted to be required for disease during *C. jejuni* infection and because neutrophil-*Campylobacter* interactions are mostly unknown, we took advantage of this observation to characterize what appeared to be a previously unidentified bacterial factor that promotes host inflammation.

From this work, we determined that CJJ81176_0779 encodes a unique *C. jejuni* effector, which we call SliP, that functions as a bacterial sirtuin and is released into neutrophils during intracellular infection. While several bacterial pathogens have been shown to hijack host sirtuins to create an intracellular environment that promotes infection, an example of a bacterial-derived sirtuin being translocated into host cells to directly alter host responses has yet to be described. In addition to the enzymatic and proinflammatory functions of SliP, we also found that the gene is more frequently present in genomes of human clinical isolates of *C. jejuni*. While the evolutionary rationale for this incidence is unknown, one explanation is that the role of SliP in neutrophil activation could lead strains that have SliP to be more inflammatory. As a result, the abundance of *sliP* in clinical isolates could be due to a detection bias since patients with more severe disease are more likely to seek medical care where those strains are likely to be isolated and sequenced. Despite this possible isolation bias, almost half of the clinical isolates we previously sequenced lack *sliP*. We felt that this observation might be explained by our later experiments where we were able to infect mice with a *sliP* mutant of *C. jejuni* but where those mice exhibit less inflammation. Therefore, we hypothesize that SliP contributes to inflammation and more severe disease in infected hosts, but it is not necessary for host colonization as SliP-deficient strains can still cause infection. Beyond its role in *C. jejuni*, we identified other bacterial pathogens that encode DUF4917 family proteins; however, they have yet to be investigated. For example, the human pathogens *L. pneumophila* and *Y. enterocolitica* encode DUF4917 proteins with homology to *C. jejuni* SliP. This observation suggests infection or disease caused by these pathogens may be similarly facilitated by the production of their bacterial-derived sirtuin.

Because we determined that SliP acts as a canonical sirtuin, we examined whether SliP inhibition could be achieved using known deacetylase inhibitors such as SB and TSA and whether treatment of infected neutrophils with these compounds could reduce activation and NET production. SB and TSA have been found to abrogate colonization of numerous bacterial pathogens and reduce host inflammation, including those caused by *S. typhimurium* (*70*, *71*), *E. coli* (*72*), *Citrobacter rodentium* (*73*, *74*), and *Staphylococcus aureus* (*75*–*78*). While the underlying molecular mechanism of this attenuation remains unclear, it may occur through inhibition of host-derived HDACs, which have been shown to be active in a variety of autoimmune disorders, including inflammatory bowel disease. Our results suggest that in addition to inhibiting the activity of host enzymes, SB may reduce inflammation by inhibiting the activities of bacterial-derived sirtuins that would otherwise alter the intracellular environment of the host to a more proinflammatory state. In the future, it would be interesting to determine whether increasing gastrointestinal butyrate, through elevated dietary fiber or altering the microbiome, can improve outcomes of campylobacteriosis.

While determining how SliP might affect neutrophil activities, we found that active SliP was translocated from *C. jejuni* into medium containing a DOC signal, that lysine deacetylation increased and NAD^+ levels decreased in a SliP-dependent manner following *C. jejuni* uptake into neutrophils, and that SliP was translocated into the neutrophil cytosol during infection. As a result, we hypothesized after release into the neutrophil, SliP targets host proteins to promote inflammatory responses. Because HDAC up-regulation and the resulting histone deacetylation have been shown to promote NETosis and host inflammation, we initially focused on SliP-dependent impacts to the acetylation status of host histones. As predicted, we found that SliP associates with histone H3 during neutrophil infection and that the presence of SliP leads to decreased histone acetylation. In addition, we observed that SliP appears to colocalize with histone H3 outside the neutrophil nucleus, which leads to the question whether SliP associates with and deacetylates histone proteins before being transported to the nucleus or whether SliP gains access to the nucleus and modifies histones associated with chromatin. This question is currently under investigation in our group. Further, since other effectors have been found to be injected into host cells through the flagellum after binding to host cells (*64*), we investigated and determined that SliP translocation depends on the flagella. Since flagella are also required for cell invasion, further work is required to determine whether SliP is actively translocated through these structures into neutrophils or whether SliP gains entry through passive means, including *C. jejuni* lysis, but current data that *C. jejuni* viability is not affected in the time it takes for SliP to associate with histones suggest that SliP is specifically translocated from intact cells. Beyond the mechanisms of translocation, we are also currently investigating whether SliP diffuses from the phagosome, a *Campylobacter*-containing vacuole that does not fuse with granules, or bacteria that are within the host cytosol. In addition, although we showed that histone H3 becomes deacetylated in a SliP-dependent manner, other PTMs could occur after deacetylation, including lysine methylation, ubiquitination, and SUMOylation (*79*–*82*).

To determine how the above activities affect animal infection, we leverage the IL-10 murine campylobacteriosis model where we found that, despite the ability of the *sliP* mutant to colonize and be shed in the feces similar to mice infected with wild-type bacteria, the bacterial burden within the spleen of *sliP* mutant–infected mice was significantly increased. We hypothesize that this observation is similar to what was observed in a previous study where NET production was shown to be involved in limiting bacterial dissemination to the spleen during *C. rodentium* infection of mice (*83*). Furthermore, we observed that *sliP* mutant–infected mice have reduced levels of proinflammatory cytokines IL-1β, IL-6, IFN-γ, KC, and TNF-α compared to wild-type–infected mice. We postulate that (i) proinflammatory cytokines could be released by activated neutrophils during infection (*84*, *85*); (ii) tissue-resident macrophages could detect citrullinated histone H3, resulting in up-regulation of proinflammatory cytokines (*86*–*88*); or (iii) influx of other leukocytes could be responsible for the increases in proinflammatory cytokines (*89*, *90*). Last, we found that inflammation and tissue pathology were dependent on the presence of SliP. While this suggests that neutrophil activation during *C. jejuni* infection is required for disease, further work needs to be conducted to determine whether SliP affects inflammatory responses in other cell types present at the site of infection, including colonocytes and macrophages. We are currently performing these studies in our group to establish the contribution of neutrophils more conclusively to disease. While fluorescence-activated cell sorting (FACS) SliP-containing neutrophils in vivo would allow us to further understand how SliP influences neutrophil physiology within the host, there are numerous technical issues with FACS neutrophils (*91*, *92*).

With further characterization of the class of bacterial effectors we identified here, the role of bacterial-driven impacts to host PTMs that are important to host-microbe interactions during infection can be better understood. Specifically in the context of *Campylobacter* infection, understanding the unique mechanisms the bacterium uses to promote infection and inflammation can lead to novel therapeutics for treating acute and chronic outcomes of infection. Several areas in human health research are actively characterizing how altered host PTMs affect various diseases, including the identification of compounds that can counteract those changes. Because of this shared interest, future research in our group will focus on the ability of these molecules to reduce disease severity during campylobacteriosis.

METHODS

Transposon nuclease screen

C. jejuni nuclease production was analyzed through a previously characterized transposon screen (*61*, *93*). Briefly, individual transposon isolates were inoculated on Mueller-Hinton (MH) agar with chloramphenicol using a 96-well replicator. After 2 days of growth, individual colonies were transferred to DNase agar using a 96-well replicator. Zones of clearance around the colonies were analyzed, and strains lacking zone of clearance were used for the secondary nuclease screen. In this secondary screen, strains were grown in MH supplemented with 0.05% DOC for 2 days under microaerobic conditions at 37°C. After 2 days of growth, cell-free supernatants were extracted and incubated with neutrophil DNA. After incubation of the DNA with supernatants for 1 hour at 37°C, tubes were chilled on ice for a minimum of 10 min. After chilling, *C. jejuni* genomic DNA was spiked into the reaction to serve as an extraction control. DNA was extracted from the reactions using 3 M sodium acetate and ethanol. After extraction, neutrophil and *C. jejuni* DNA were amplified through qPCR using *GAPDH* and *mapA* specific primers, respectively. Strains lacking significant differences between nondegraded DNA and *C. jejuni* supernatant were deemed lacking secreted nuclease production.

Abundance of SliP within environmental and clinical isolates

Environmental and clinical isolates of *C. jejuni* were isolated from a previous study (*54*). Whole genomes were uploaded to KBase, and their genomes were annotated to the 81-176 wild-type genome. After the genomes were annotated, amino acid homology was performed, with the minimum homology set to 75%. For statistical analysis, a two-sided chi-square test was performed.

Operonic PCRs of the *sliP* operon

To determine whether other genes within the gene neighborhood of *sliP* were cotranscribed, primers were designed within the intergenic regions of genes upstream and downstream of *sliP*. *C. jejuni* genomic DNA was used to ensure primers amplified a single product predicted to be approximately 500 base pairs or less. After, RNA was extracted from *C. jejuni* incubated with neutrophils using an RNeasy Mini Kit. cDNA was synthesized from the RNA using reverse transcriptase (+), and mock reverse transcriptase (−) was performed to check for genomic DNA contamination. PCRs were performed on samples, then ran on a 1% agarose gel, and visualized using ethidium bromide and a ultraviolet imager.

Phylogenetic analysis of DUF4917 family proteins

To understand the homology of SliP with other members of the DUF4917 family, an amino acid BLAST was performed, excluding *Campylobacter* spp. DUF4917 proteins. From this BLAST search, amino acids were pulled from the top 14 percent homology organisms. The annotated amino acids were then aligned using multiple sequence alignment using T-Coffee (EMBL-EFI) with a ClustalW output. From this, a neighbor-joining tree without distance correction cladogram was produced.

Bacterial cultures and culture conditions

C. jejuni 81-176 strain DRH212 was stored at −80°C in MH broth supplemented with 20% glycerol. In this study, nonpolar deletions and plasmid-borne strains of *sliP* were constructed in wild-type *C. jejuni* DRH212 as previously described (*94*). All strains were routinely grown for 24 hours on selective medium [10% sheep's blood, cefoperazone (40 μg/ml), cycloheximide (100 μg/ml), trimethoprim (10 μg/ml), and vancomycin (100 μg/ml)] before passing onto MH agar containing 10% sheep's blood and trimethoprim (10 μg/ml) at 37°C under microaerobic conditions (85% N_2, 10% CO_2, and 5% O_2) for an additional 24 hours. *E. coli* expression strain C3013 containing pQE30-*sliP* and pQE-30-$sliP_{G26A}$ were constructed as previously described (*95*). *E. coli* strains were stored in Luria-Bertani (LB) broth supplemented with 20% glycerol at −80°C and grown shaking at 37°C in LB broth supplemented with ampicillin for purification as described below.

Isolation of primary human neutrophils

Neutrophils were isolated as previously described (*7*, *97*). Briefly, 10 ml of blood was drawn from healthy donors into heparinized Vacutainer tubes and mixed 1:1 with sterile 1× phosphate-buffered saline (PBS) (approval UTK IRB-18-04604-XP) (*97*). After mixing, 10 ml of lymphocyte separation medium was underlaid. Following centrifugation at 1400 rpm for 30 min, the top layers were aspirated off, leaving the red blood cell and neutrophil pellet. Pellets were resuspended in 20 ml of Hanks′ balanced salt solution and 20 ml of 3% dextran in 0.9% NaCl. After incubating at room temperature for 20 min, the upper layer was transferred to a new tube. Following centrifugation at 400*g* for 5 min and aspiration of the supernatant, the pellet was washed with 20 ml of ice-cold 0.2% NaCl and 20 ml of ice-cold 1.6% NaCl two times. Following the final aspiration, the neutrophil pellet was resuspended in 10 ml of RPMI 1640. Neutrophil viability and counts were performed through Trypan blue stain.

Protein induction and native purification of SliP

Protein induction and purification were performed as previously described (*61*, *95*). Briefly, *E. coli* strains C3013 encoding SliP, $SliP_{G26A}$, or empty pQE-30 vector were grown overnight in LB broth containing ampicillin (100 μg/ml) at 37°C shaking. Cultures were then back-diluted by adding 1 ml of overnight culture in 100 ml of LB broth containing ampicillin (100 μg/ml). Culture was grown at 37°C shaking for 2 hours before spiking in 100 μM isopropyl-β-D-thiogalactopyranoside to induce protein expression. Cultures were allowed to incubate for an additional 2 hours at 37°C shaking. After incubation, cells were pelleted at 2147 rcf for 10 min. After centrifugation, the pellets were resuspended in lysis buffer [50 mM NaH_2PO_4, 300 mM NaCl, and 10 mM imidazole (pH 8.0)] before sonication on ice (six rounds of 15 s each at 45 A). Cell lysates were then pelleted at 2147 rcf for 10 min before incubating the resultant supernatant with washed Ni-NTA for 1 hour at 4°C rocking. After the incubation, the SliP resin was packed in a 20-ml chromatography column before it was washed three times with 4 ml of wash buffer [50 mM NaH_2PO_4, 300 mM NaCl, and 20 mM imidazole (pH 8.0)] and eluted in three 750 μl fractions of elution buffer [50 mM NaH_2PO_4, 300 mM NaCl, and 250 mM imidazole (pH 8.0)]. Each wash and elution fraction were diluted 1:1 with a Laemmli buffer containing β-mercaptoethanol and boiled for 10 min. Ten microliters of lysate samples were loaded onto a 12.5% SDS–polyacrylamide gel electrophoresis (PAGE) gel and run for 1 hour at 150 V at room temperature and stained with Coomassie to ensure protein purification (37 kDa). Elution fractions were then pooled and dialyzed using a dialysis buffer [200 mM NaCl, 2 mM dithiothreitol, and 20 mM Hepes buffer (pH 7.5)] three times at 4°C spinning. After dialysis, protein was collected from the dialysis cassette using a syringe and stored at 4°C until future use.

To generate C terminally 6x His-tagged SliP, a 6x His tag was incorporated onto the primers to amplify *sliP*. The amplified *sliP* was put into pGemT plasmid and then sequenced through Sanger sequencing. Once sequenced, pGemT-*sliP* was electroporated into C3013. C-terminal 6x His tagged SliP was purified as previously described.

Site-directed mutagenesis to create $sliP_{G26A}$

To create $sliP_{G26A}$ for complementation and protein purification, the single-nucleotide polymorphism (SNP) was generated using primer-derived SNP. To do this, the SNP was generated in the forward primer and then used stitching overlapping extensions to generate the full-length sliP encoding the G26A mutation. The mutation was confirmed through PCR and Sanger sequencing technology. Single–amino acid substitution of $SliP_{G24A}$ and double–amino acid substitution of $SliP_{G24A,G26A}$ were generated through GenScript with tailed Bam H1 cut sites. These inserts were introduced into pQE30 and pECO102 for protein purification and complementation, respectively.

Detection of in vitro and in vivo lysine deacetylation

Quantification of in vitro and in vivo lysine deacetylation was performed using the BioVision InSitu HDAC Activity Fluorometric Assay Kit (catalog no. K339-100). For in vitro quantification, 10 ng of purified SliP was incubated in the presence of HDAC substrate (acetylated lysine side chain) with 5 mM NAD^+ and 20 μM $ZnCl_2$ at 37°C. For in vivo quantification, 10^5 neutrophils were incubated with 10^6 *C. jejuni* to a final volume of 150 μl containing the HDAC substrate, and the cells were infected as previously described (*7*). After the allotted amount of time, developer and HDAC assay buffer were added to 100 μl of reaction mixture (with the other 50 μl being used for the NAD^+ hydrolysis assay described below) and were incubated for 30 min at 37°C. After incubation, fluorescence was read using a BioTek Synergy microplate reader at 368/442 nm wavelength. A deacetylated substrate standard curve was additionally run and plotted with fluorescence. Once plotted, the amount of deacetylated lysine residues was calculated.

Quantification of NAD^+ and NADH within neutrophils and supernatants

The abundance of NAD^+ and NADH in vitro and in vivo was performed using the Promega NAD/NADH-Glo Assay. All reagents used for this assay were brought to room temperature before use. For the in vitro NAD^+ hydrolysis assay, 5 mM pure NAD^+ was added to the reaction as described above in the lysine deacetylation assay. After deacetylation, the NAD/NADH-Glo detection reagent was made as described by the manufacturer. In a white welled plate, 50 μl from the lysine deacetylation reaction mixture was combined with 50 μl of detection reagent. The plate was incubated at 37°C for 30 min while shaking. After incubation, luminescence was read using a BioTek Synergy microplate reader. For quantification of intracellular NAD^+ and NADH, neutrophils were infected with their respective strain for the allotted amount of time under microaerobic conditions at 37°C to a final volume of 50 μl. Neutrophils were then lysed by adding 50 μl of RPMI 1640 containing 1% dodecyltrimethylammonium bromide. To measure NAD^+, 50 μl of the reaction mixture was allotted and mixed with 25 μl of 0.4 N of hydrochloric acid and incubated at 60°C for 15 min. After the incubation, the samples were cooled at room temperature for 10 min. Then, 25 μl of Trizma base was added to the reaction mixture. Last, 100 μl of detection reagent was added and incubated as previously described, and luminescence was read as previously described. For NADH quantification, 50 μl of the cell lysis solution was incubated at 60°C for 15 min. The samples were cooled at room temperature for 10 min. Then, 50 μl of HCl/Trizma base solution was added to the reaction mixture. Last, 100 μl of detection reagent was added and incubated as previously described, and luminescence was read as previously described. Along with each experiment, a known concentration standard curve for NAD^+ and NADH was constructed to calculate the concentration of each small molecule.

SliP-CyaA neutrophil translocation assay

To determine whether SliP is translocated into neutrophils, adenylate cyclase translational fusions were produced at the C terminus of *sliP*, *heuR*, and *ciaB* (*98*). For each infection, 10^6 neutrophils were incubated with wild-type or Δ*flgE C. jejuni* strains harboring pECO102 encoding *sliP-cyaA*, *heuR-cyaA*, or *ciaB-cyaA* at a multiplicity of infection of 10 for 3 hours under microaerobic conditions at 37°C. In addition, actin polymerization was chemically blocked with 2 μM CD for 1 hour before bacterial infection under microaerobic conditions at 37°C. Cells were lysed with 0.1 M HCl, and the direct ELISA was performed as according to the manufacturer′s protocol (Enzo). All experiments were additionally done with wild-type and Δ*flgE C. jejuni* and CD-incubated neutrophils without the addition of *cyaA*. These values can be taken out of the respective treatment groups.

Analysis of *C. jejuni* NET induction by flow cytometry

Flow cytometry detection of *C. jejuni*–induced NETs was performed as previously described (*7*, *96*). Briefly, *C. jejuni* strains were resuspended in RPMI 1640 and incubated with neutrophils for 3 hours under microaerophilic conditions at an equal multiplicity of infection of 50:1 (bacteria:neutrophil). Following incubation, these reactions were aliquoted into wells of a 96-well plate and centrifuged at 400*g*. Pelleted cells were washed three times with sterile 1× PBS cells before incubation with Live/Dead near-infrared stain for 25 min at room temperature. After incubation, cells were blocked with 1% goat serum for 10 min and then incubated with CD11b and MPO antibodies for 30 min (*99*). Cells were subsequently fixed in the fixation buffer for 10 min at room temperature and stored at 4°C until flow cytometry analysis. Samples were analyzed using an LSR II flow cytometer, and data were processed using BD FlowJo software. Statistical analysis was performed using unpaired *t* tests and significance inferred at $P < 0.05$.

Analysis of *C. jejuni* NET induction by SYTOX assay

SYTOX NET quantification was performed as previously described (*7*, *96*). Briefly, Following the *C. jejuni* NET induction described above, cells were added to wells of black 96-well plates and centrifuged at 400*g*. Supernatants were discarded, and 1.0 μM SYTOX Green was added to each sample and incubated under microaerobic conditions at 37°C for 1 hour (*100*). After incubation, cells were centrifuged at 400*g*, and the supernatant was discarded. The cells were washed once with 1× PBS and then resuspended in 100 μl of 1× PBS. SYTOX fluorescence was measured at 504/523 nm using a BioTek Synergy microplate reader. Statistical analysis was performed using unpaired *t* tests and significance inferred at $P < 0.05$.

Western blot analysis of NET products

Detection of NET components via Western blot was performed as previously described (*7*). Briefly, NETs were induced as described above, and cells from healthy volunteers were lysed with Laemmli buffer with β-mercaptoethanol and boiled for 10 min. Ten microliters of whole-cell lysate samples were loaded onto a 12.5% SDS-PAGE gel and run for 1.25 hours at 140 V at room temperature. Separated proteins were transferred to nitrocellulose membranes (GE Healthcare, catalog no. 10600011) for 1.5 hours at 0.25 A using a semidry transfer apparatus. Membranes were blocked in 5% milk in tris-buffered saline (TBS)–T for 60 min shaking. To probe proteins of interest, 1:500 dilution rabbit anti-*C. jejuni* SliP (Cocalico Biologicals), 1:5000 dilution rabbit anti-human Lcn2 (Invitrogen, catalog no. 702248), 1:1000 dilution rabbit anti-human PAD4 (Thermo Fisher Scientific, catalog no. PA5-12236), 1:1000 dilution rabbit anti-human histone H3 (Active Motif, catalog no. 61799), 1:1000 dilution rabbit anti-human acetyl histone H3 (Active Motif, catalog no. 39040), and 1:500 dilution mouse anti-human β-actin (Cell Signaling Technology, catalog no. 4970) were incubated on individual membranes for 1 hour at room temperature with shaking. Membranes were subsequently washed three times with filtered TBS-T for 5 min each. Proteins of interest were detected using a 1:2000 dilution of appropriate horseradish peroxidase–conjugated secondary antibodies in 15 ml of 5% milk in TBS-T and incubated for 45 min at room temperature with shaking. Membranes were then washed three times with filtered TBS-T, shaking for 5 min each. After the final wash, membranes were developed with a solution containing 5 ml of peroxide and 5 ml of luminol/enhancer solution (Thermo Fisher Scientific, catalog no. 34580) and incubated for 5 min at room temperature with shaking. A *C. jejuni* negative control was also performed to ensure that there was no cross-reactivity and no detection of proteins was noted. Chemiluminescent bands were imaged using the ChemiDoc-It Imager, and densitometry measurements were made using NIH ImageJ software. Statistical analysis was performed using unpaired *t* tests and significance inferred at $P < 0.05$.

Production of rabbit anti-SliP antibodies

To generate anti-SliP antibodies, SliP was purified as previously described. Then, 500 μg of SliP were run on an SDS-PAGE gel and allowed to run to separate out whole-cell *E. coli* lysates. After the gel ran, the gel was stained with Coomassie blue and then destained to view protein on the gel. After the gel was destained, the bands containing SliP were excised and placed in sterile water and shipped to Cocalico Biologicals Inc. Two rabbits were initially inoculated with a minimum of 50 μg of SliP in Incomplete Freund′s via subcutaneous injection. After 2 and 3 weeks after inoculation, the rabbits were boosted with a minimum of 50 μg of SliP in Incomplete Freund′s via subcutaneous injection or intramuscular injection at multiple sites. After 2 weeks following the 3 weeks after inoculation booster, rabbits were bled, and serum was saved for laboratory use. Two weeks following the test bleed, the rabbits were boosted with a minimum of 50 μg of SliP in Incomplete Freund′s via subcutaneous injection or intramuscular injection at multiple sites. One week following the last booster, rabbits were bled, and serum was saved for laboratory use. Rabbit serum was aliquoted in 1 ml of aliquots and frozen at −20°C until Western blot or coimmunoprecipitation was performed.

Neutrophil acetone protein powder for antibody cleaning

To clean the serum for nonspecific binding, Δ*sliP*-infected neutrophils were incubated as previously described in this manuscript. After incubation, cells were washed three times with 1× PBS. After washes, cells were resuspended in 0.9% NaCl to a ratio of 1 ml of salt solution for 1 g of cells. Next, the cells were incubated on ice for 5 min. After incubation, −20°C chilled 100% acetone was added to the cells at a 4:1 ratio and incubated at 0°C rocking for 30 min. After rocking incubation, tubes were centrifuged at 10,000*g* for 10 min at 4°C, where supernatant was discarded. The pellet was then resuspended in −20°C chilled 100% acetone, mixed vigorously, and then incubated at 0°C for 10 min. Tubes

were then centrifuged at 10,000*g* for 10 min at 4°C, where supernatant was discarded. Once the supernatant was discarded, the pellet was transferred to a clean piece of filter paper and allowed to air-dry. Once dried, the acetone protein powder was stored in an airtight container at 4°C until use (*101*). To use, powder was incubated with anti-SliP serum at a concentration of 1%. Serum was then incubated for 30 min at 4°C. After incubation, the serum was centrifuged at 10,000*g* for 10 min at 4°C. After centrifugation, the supernatant was saved and stored at −20°C until usage.

Reverse transcription qPCR analysis of gene expression

For extracting neutrophil RNA, RNA was extracted using a QIAGEN RNeasy Kit per the manufacturer′s protocol. RNA samples were eluted from the kit columns using nuclease-free water and stored at −20°C. All RNA samples were then DNase-treated, and pure RNA was clean and concentrated using a kit (Zymo). Each sample was tested for DNA contamination through standard PCR. cDNA was then produced from DNA-clear RNA using the Bio-Rad iScript kit using the manufacturer′s protocol. Primers specific to *sliP*, *HDAC1*, *HDAC2*, *HDAC3*, *SIRT1*, *SIRT2*, *SIRT6*, *SIRT7*, *GCN5*, *PCAF*, *P300*, *CBP*, *SRC1*, *ACTR*, *TAF11250*, *TFIIIC90*, *GAPDH*, *and rpoA* were designed using PrimerQuest (IDT) (table S1). The abundance of each gene expression was determined using the iTaq Universal SYBR green master mix (Bio-Rad). Threshold values (C_T) were used to calculate the $\Delta\Delta C_T$ using *GAPDH* as the internal control for human genes. For neutrophil gene expression, abundance was normalized to neutrophils in medium alone (uninfected).

In vitro immunofluorescence microscopy

Cocultures were completed in wells containing sterile 12 mm poly-L-lysine–coated coverslip (Corning, NY), and cells were fixed in a solution of 2% paraformaldehyde and 2.5% glutaraldehyde in 0.1 M sodium cacodylate buffer (pH 7.4) (Electron Microscopy Sciences, Hatfield, PA). Coverslips were washed thrice with TBS (pH 7.4) before permeabilizing with 0.25% Triton X-100. Samples were then incubated in blocking buffer (TBS with 10% bovine serum albumin) for 120 min, followed by overnight incubation at 4°C with a 1:200 dilution of the polyclonal rabbit serum and antibodies for histone H3 (final concentration of 2.5 μg/ml; Sigma-Aldrich, SAB4200651) in blocking buffer. Samples were washed in blocking buffer thrice and stained with 1:1000 dilution of alpaca anti-rabbit immunoglobulin G (IgG) nano (VHH) recombinant secondary antibody conjugated with Alexa Fluor 647 (Invitrogen, SA5-10327), goat anti-mouse IgG conjugated with Alexa Fluor Plus 488 (final concentration of 5 μg/ml; Invitrogen, A32723), and 10 μM Hoechst 33342 for 120 min at room temperature. Coverslips were washed twice in blocking buffer and twice in TBS before mounting with ProLong Glass Antifade Mountant (Invitrogen, P36982). Samples were visualized with a Zeiss LSM 710 META inverted laser scanning confocal microscope in part using the Vanderbilt Cell Imaging Shared Resource. Presented images are three-dimensional reconstructions of z-stacked images.

Coimmunoprecipitation of histone H3 and SliP

Neutrophils were purified and infected with *C. jejuni* wild-type, Δ*sliP*, and complement strains as previously described. After non-NETosing condition incubation, cells were fixed and cross-linked by the addition of paraformaldehyde to a final concentration of 4% and incubated for 10 min at room temperature. After cross-linking, glycine was added to a final concentration of 125 mM and incubated for 5 min, shaking. The cells were then washed three times with ice-cold 1× PBS. After the final wash, the cells were lysed using 750 μl of radioimmunoprecipitation assay buffer [150 mM NaCl, 1% NP-40, 0.5% DOC, 0.1% SDS, and 50 mM Tris (pH 7.4)]. After lysis of the cells, the samples were centrifuged at 14,000*g* for 10 min at 4°C. After centrifugation, the supernatant was pulled off and placed in a sterile 1.5 ml Eppendorf tube. Next, the histone H3 antibody was added to the supernatant at a dilution of 1:1000. The supernatant-antibody solution was incubated overnight at 4°C rocking. After the incubation, 10 μl of protein A beads were added to each sample and incubated at 4°C for 3 hours rocking. After incubation, the tubes were placed on a magnet to pull down beads conjugated to the antibody-protein complexes. The conjugated beads were washed three times with radioimmunoprecipitation assay buffer, using a magnet at 4°C each time. After the last wash, the proteins were eluted by adding Laemmli buffer with β-mercaptoethanol and boiled for 10 min. After the boiling, the tubes were placed on a magnet to discard the protein A agarose beads. Eluted proteins in Laemmli buffer were stored at −20°C until Western blot analysis as previously described.

Infection of IL-10$^{-/-}$ mice with *C. jejuni*

All animal protocols were approved by the Institutional Animal Care and Use Committee at the University of Tennessee–Knoxville (UTK IACUC protocol #2885). As previously described, *C. jejuni* DRH212 and Δ*sliP* were grown on *Campylobacter*-specific medium and Gram stained to ensure culture purity before inoculation (*8*). This culture was streaked on *Campylobacter*-selective medium and incubated at 37°C under microaerophilic conditions for 48 hours. Suspensions of *C. jejuni* 81-176 were made in sterile PBS and diluted to an optical density at 600 nm of 10. Five female-specific pathogen-free 8-to-12-week-old IL-10$^{-/-}$ C57BL/6 mice were gavaged with a single dose of 10^{10} colony-forming units (CFUs) per mouse of *C. jejuni* wild-type strain 81-176 or the Δ*sliP* mutant. In addition, five female mice were mock infected with sterile 1× PBS. Each day for 10 days, approximately 20 mg of feces from one sample from each animal were immediately weighed out and diluted 1:100 in PBS. The remaining samples were immediately frozen at −80°C. Diluted samples were further serially diluted in PBS to 10^{-8}, and 100 μl of each dilution was plated on *Campylobacter*-specific medium. The plates were then incubated at 37°C under microaerophilic conditions for 48 hours before *Campylobacter* loads were determined. After 10 days after infection, blood was collected by cardiac puncture, and mice were euthanized as previously described. From the blood, serum was collected and frozen at −20°C for further analyses. Ceca, colons, and spleens were excised from each mouse and placed in sterile 1× PBS. Colons were additionally rolled in Swiss Rolls and placed in formalin solution before being fixed in paraffin. To determine bacterial load in these tissues, ground tissue was weighed and diluted 1:100 in PBS. Diluted samples were further serially diluted in PBS to 10^{-8}, and 100 μl of each dilution was plated on *Campylobacter*-specific medium.

Histological analysis of murine intestinal tissue during *C. jejuni* infection

Pathology scoring for intestinal tissue was performed as previously described (*7*). The terminal 1 cm of the murine colon was removed following euthanasia, and the lumen was washed five times with 1 ml of sterile, cold 1× PBS. Tissue was placed in 10% buffered formalin and fixed for 4 hours at room temperature. Fixed tissue was embedded in formalin, and 4 μm sections were stained with hematoxylin and eosin (H&E). Stained slides were visualized through bright-field microscopy, and representative images were presented. Inflammation scoring was performed as described in a blind manner, noting edema, presence of blood, hyperplasia, loss of goblet cells, epithelia raggedness, and neutrophil infiltration (*67*). Statistical analysis was performed using a nonparametric Mann-Whitney *U* test.

Quantification of proinflammatory cytokines from murine serum

Murine cytokines from sera were quantified using the BioLegend LEGENDplex Anti-Virus response panel in a V-bottom plate per the manufacturer′s guidelines. Briefly, serum was plated, alongside a standard curve of known concentrations for various cytokines. Assay buffers were added to each well, along with mixed beads that had been sonicated in water baths and vortexed to ensure homogeneity. The plate was sealed, wrapped in aluminum foil, and shook on a plate shaker at 800 rpm for 2 hours at room temperature. After incubation, the plate was centrifuged at 250*g* for 5 min using a swinging basket. After centrifugation, the plate seal was removed, and the supernatant was immediately flicked off into a bucket. The wells were then washed using the manufacturer′s wash buffer twice before the detection antibody was added to each well. The plate was sealed and covered in aluminum foil and shook on a plate shaker at 800 rpm for 1 hour at room temperature. After incubation, a streptavidin-phycoerythrin solution was added to the wells, and the plate was sealed and wrapped in aluminum foil, where it incubated on a plate shaker at 800 rpm for 30 min at room temperature. After incubation, the plate was centrifuged and washed as previously described. Once the preparation was complete, the samples were resuspended in wash buffer until flow cytometry analysis. Samples were analyzed using an LSR II flow cytometer, and data were processed using the BioLegend LEGENDplex data analysis software. Cytokine concentrations were determined due to the standard curve generated by standard bead concentrations.

In vivo fluorescence microscopy of mouse tissue samples

Parrafin-embedded mouse tissues were stained for fluorescence microscopy as previously described (*7*, *102*, *103*). Briefly, slides containing slices of paraffin-embedded tissues were digested in three rounds of xylene washes for 5 min, followed by a final wash in xylene for 10 min at room temperature. Afterward, slides were washed with two rounds of 5-min washes with 100, 95, 70, and 50% ethanol each at room temperature. After the final ethanol wash, slides were rehydrated in deionized water by incubating for 5 min twice at room temperature. After rehydration, slides were incubated in R Universal Epitope Recovery Buffer (Electron Microscopy Sciences) at 50°C for 90 min. After incubation, slides were then washed with deionized water three times for 5 min each. The slides were then washed with TBS (pH 7.4) three times for 5 min each at room temperature. Samples were then permeabilized for 5 min with 0.5% Triton X-100 in TBS at room temperature, followed by three washes with TBS for 5 min each at room temperature. Samples were then blocked with TBS with 10% bovine serum albumin for 30 min at room temperature. After blocking, samples were then incubated with 1:20 dilution of histone H3, 1:20 acetyl-histone H3, 1:50 *Campylobacter*, and 1:100 MPO antibodies overnight at room temperature covered in the dark. After overnight incubation, slides were washed three times with TBS for 5 min each at room temperature. After the final wash, the samples were stained with 5 μM Hoechst 33342 for 30 min at room temperature. After the incubation, slides were washed three times with TBS for 5 min each at room temperature. After the final wash, the slides were air-dried and coverslipped using Mowiol. Tissues were visualized with a Nikon E600 Eclipse at the Advanced Microscopy and Imaging Center at the University of Tennessee. Images presented are composites of z-stacked images.

Purification of immune cells from murine colon tissues for coimmunoprecipitation

$CD45^+$ immune cells were purified from the colons of uninfected, wild-type–, and Δ*sliP*-infected mice per manufacturer′s guidelines (MojoSort BioLegend). After purification of $CD45^+$ cells, cells were incubated in formalin to cross-link protein complexes at 4°C. The histone H3 coimmunoprecipitation was performed as previously described, with samples stored at −20°C until Western blot analysis was performed.

Supplementary Materials

This PDF file includes:

Figs. S1 to S12
Tables S1 and S2
Legends for movies S1 and S2
References

Other Supplementary Material for this manuscript includes the following:

Movies S1 and S2

REFERENCES AND NOTES

1. S. M. Man, The clinical importance of emerging *Campylobacter* species. *Nat. Rev. Gastroenterol. Hepatol.* **8**, 669–685 (2011).
2. World Health Organization. *WHO Estimates of the Global Burden of Foodborne Diseases: Foodborne Disease Burden Epidemiology Reference Group 2007–2015* (World Health Organization, 2015).
3. S. M. Callahan, C. G. Dolislager, J. G. Johnson, The host cellular immune response to infection by *Campylobacter* spp. and its role in disease. *Infect. Immun.* **89**, e0011621 (2021).
4. K. L. Reti, L. D. Tymensen, S. P. Davis, M. W. Amrein, A. G. Buret, *Campylobacter jejuni* increases flagellar expression and adhesion of noninvasive *Escherichia coli*: Effects on enterocytic toll-like receptor 4 and CXCL-8 expression. *Infect. Immun.* **83**, 4571–4581 (2015).
5. J. Silva, D. Leite, M. Fernandes, C. Mena, P. A. Gibbs, P. Teixeira, *Campylobacter* spp. as a foodborne pathogen: A review. *Front. Microbiol.* **2**, 200 (2011).
6. K. T. Young, L. M. Davis, V. J. DiRita, *Campylobacter jejuni*: Molecular biology and pathogenesis. *Nat. Rev. Microbiol.* **5**, 665–679 (2007).
7. S. Callahan, R. S. Doster, J. W. Jackson, B. R. Kelley, J. A. Gaddy, J. G. Johnson, Induction of neutrophil extracellular traps by *Campylobacter jejuni*. *Cell. Microbiol.* **22**, e13210 (2020).
8. J. M. Shank, B. R. Kelley, J. W. Jackson, J. L. Tweedie, D. Franklin, S. M. Damo, J. A. Gaddy, C. N. Murphy, J. G. Johnson, The host antimicrobial protein calgranulin C participates in the control of *Campylobacter jejuni* growth via zinc sequestration. *Infect. Immun.* **86**, e00234-18 (2018).

9. N. B. Sørensen, H. L. Nielsen, K. Varming, H. Nielsen, Neutrophil activation by *Campylobacter concisus*. *Gut Pathog.* **5**, 17 (2013).
10. X. Sun, D. Threadgill, C. Jobin, *Campylobacter jejuni* induces colitis through activation of mammalian target of rapamycin signaling. *Gastroenterology* **142**, 86–95.e5 (2012).
11. X. Sun, B. Liu, R. B. Sartor, C. Jobin, Phosphatidylinositol 3-kinase-γ signaling promotes *Campylobacter jejuni* –induced colitis through neutrophil recruitment in mice. *J. Immunol.* **190**, 357–365 (2013).
12. B. Barneda-Zahonero, M. Parra, Histone deacetylases and cancer. *Mol. Oncologia* **6**, 579–589 (2012).
13. P. Hamminger, R. Rica, W. Ellmeier, Histone deacetylases as targets in autoimmune and autoinflammatory diseases. *Adv. Immunol.* **147**, 1–59 (2020).
14. M. R. Shakespear, M. A. Halili, K. M. Irvine, D. P. Fairlie, M. J. Sweet, Histone deacetylases as regulators of inflammation and immunity. *Trends Immunol.* **32**, 335–343 (2011).
15. A. Bhaskar, S. Kumar, M. Z. Khan, A. Singh, V. P. Dwivedi, V. K. Nandicoori, Host sirtuin 2 as an immunotherapeutic target against tuberculosis. *eLife* **9**, e55415 (2020).
16. M. Gogoi, K. Chandra, M. Sarikhani, R. Ramani, N. R. Sundaresan, D. Chakravortty, *Salmonella* escapes adaptive immune response via SIRT2 mediated modulation of innate immune response in dendritic cells. *PLOS Pathog.* **14**, e1007437 (2018).
17. M. E. Pennini, S. Perrinet, A. Dautry-Varsat, A. Subtil, Histone methylation by NUE, a novel nuclear effector of the intracellular pathogen chlamydia trachomatis. *PLOS Pathog.* **6**, e1000995 (2010).
18. J. M. Pereira, C. Chevalier, T. Chaze, Q. Gianetto, F. Impens, M. Matondo, P. Cossart, M. A. Hamon, Infection reveals a modification of SIRT2 critical for chromatin association. *Cell Rep.* **23**, 1124–1137 (2018).
19. D. Ribet, P. Cossart, Post-translational modifications in host cells during bacterial infection. *FEBS Lett.* **584**, 2748–2758 (2010).
20. D. Ribet, P. Cossart, Pathogen-mediated posttranslational modifications: A re-emerging field. *Cell* **143**, 694–702 (2010).
21. M. Rolando, S. Sanulli, C. Rusniok, L. Gomez-Valero, C. Bertholet, T. Sahr, R. Margueron, C. Buchrieser, *Legionella pneumophila* effector RomA uniquely modifies host chromatin to repress gene expression and promote intracellular bacterial replication. *Cell Host Microbe* **13**, 395–405 (2013).
22. V. Bernal, S. Castaño-Cerezo, J. Gallego-Jara, A. Écija-Conesa, T. de Diego, J. L. Iborra, M. Cánovas, Regulation of bacterial physiology by lysine acetylation of proteins. *N. Biotechnol.* **31**, 586–595 (2014).
23. J. Luu, V. J. Carabetta, Contribution of N^{ε}-lysine acetylation towards regulation of bacterial pathogenesis. *mSystems* **6**, e00422-21 (2021).
24. D. Salomon, K. Orth, What pathogens have taught us about posttranslational modifications. *Cell Host Microbe* **14**, 269–279 (2013).
25. L. Mariño-Ramírez, M. G. Kann, B. A. Shoemaker, D. Landsman, Histone structure and nucleosome stability. *Expert Rev. Proteomics* **2**, 719–729 (2005).
26. M. A. Glozak, E. Seto, Histone deacetylases and cancer. *Oncogene* **26**, 5420–5432 (2007).
27. S. K. Kurdistani, M. Grunstein, Histone acetylation and deacetylation in yeast. *Nat. Rev. Mol. Cell Biol.* **4**, 276–284 (2003).
28. C. B. Greer, Y. Tanaka, Y. J. Kim, P. Xie, M. Q. Zhang, I. H. Park, T. H. Kim, Histone deacetylases positively regulate transcription through the elongation machinery. *Cell Rep.* **13**, 1444–1455 (2015).
29. M. Haberland, R. L. Montgomery, E. N. Olson, The many roles of histone deacetylases in development and physiology: Implications for disease and therapy. *Nat. Rev. Genet.* **10**, 32–42 (2009).
30. I. Nusinzon, C. M. Horvath, Histone deacetylases as transcriptional activators? Role reversal in inducible gene regulation. *Sci. STKE* **2005**, re11 (2005).
31. H. R. Gatla, Y. Zou, M. M. Uddin, I. Vancurova, Epigenetic regulation of interleukin-8 expression by class I HDAC and CBP in ovarian cancer cells. *Oncotarget* **8**, 70798–70810 (2017).
32. T. Marumo, K. Hishikaw, M. Yoshikawa, J. Hirahashi, S. Kawachi, T. Fujita, Histone deacetylase modulates the proinflammatory and -fibrotic changes in tubulointerstitial injury. *Am. J. Physiol.-Ren. Physiol.* **298**, F133–F141 (2010).
33. H. Zhu, L. Shan, P. W. Schiller, A. Mai, T. Peng, Histone deacetylase-3 activation promotes tumor necrosis factor-α (TNF-α) expression in cardiomyocytes during lipopolysaccharide stimulation. *J. Biol. Chem.* **285**, 9429–9436 (2010).
34. Z. Chen, C. Liu, Y. Jiang, H. Liu, L. Shao, K. Zhang, D. Cheng, Y. Zhou, W. Chong, HDAC inhibitor attenuated NETs formation induced by activated platelets in vitro, partially through downregulating platelet secretion. *Shock* **54**, 321–329 (2020).
35. H. J. Hamam, N. Palaniyar, Histone deacetylase inhibitors dose-dependently switch neutrophil death from NETosis to apoptosis. *Biomolecules* **9**, 184 (2019).
36. V. Poli, V. P.-Y. Ma, M. D. Gioia, A. Broggi, M. Benamar, Q. Chen, R. Mazitschek, S. J. Haggarty, T. A. Chatila, J. M. Karp, I. Zanoni, Zinc-dependent histone deacetylases drive neutrophil extracellular trap formation and potentiate local and systemic inflammation. *iScience* **24**, 103256 (2021).
37. A. S. Rohrbach, D. J. Slade, P. R. Thompson, K. A. Mowen, Activation of PAD4 in NET formation. *Front. Immunol.* **3**, 360 (2012).
38. M. Leshner, S. Wang, C. Lewis, H. Zheng, X. A. Chen, L. Santy, Y. Wang, PAD4 mediated histone hypercitrullination induces heterochromatin decondensation and chromatin unfolding to form neutrophil extracellular trap-like structures. *Front. Immunol.* **3**, 307 (2012).
39. Y. P. Silva, A. Bernardi, R. L. Frozza, The role of short-chain fatty acids from gut microbiota in gut-brain communication. *Front. Endocrinol.* **11**, 25 (2020).
40. R. B. Canani, Potential beneficial effects of butyrate in intestinal and extraintestinal diseases. *World J. Gastroenterol.* **17**, 1519–1528 (2011).
41. M. T. Siddiqui, G. A. Cresci, The immunomodulatory functions of butyrate. *J. Inflamm. Res.* **14**, 6025–6041 (2021).
42. L. Yin, G. Laevsky, C. Giardina, Butyrate suppression of colonocyte NF-κB activation and cellular proteasome activity. *J. Biol. Chem.* **276**, 44641–44646 (2001).
43. D. M. Vigushin, S. Ali, P. E. Pace, N. Mirsaidi, K. Ito, I. Adcock, R. C. Coombes, Trichostatin A is a histone deacetylase inhibitor with potent antitumor activity against breast cancer in vivo. *Clin. Cancer Res.* **7**, 971–976 (2001).
44. W. You, C. Steegborn, Structural basis of sirtuin 6 inhibition by the hydroxamate trichostatin A: Implications for protein deacylase drug development. *J. Med. Chem.* **61**, 10922–10928 (2018).
45. H. Kankaanranta, M. Janka-Junttila, P. Ilmarinen-Salo, K. Ito, U. Jalonen, M. Ito, I. M. Adcock, E. Moilanen, X. Zhang, Histone deacetylase inhibitors induce apoptosis in human eosinophils and neutrophils. *J. Inflamm.* **7**, 9 (2010).
46. S. Toki, K. Goleniewska, S. Reiss, W. Zhou, D. C. Newcomb, M. H. Bloodworth, M. T. Stier, K. L. Boyd, V. V. Polosukhin, S. Subramaniam, R. S. Peebles Jr., The histone deacetylase inhibitor trichostatin A suppresses murine innate allergic inflammation by blocking group 2 innate lymphoid cell (ILC2) activation. *Thorax* **71**, 633–645 (2016).
47. B. Milne-Davies, C. Helbig, S. Wimmi, D. W. C. Cheng, N. Paczia, A. Diepold, Life after secretion—*Yersinia enterocolitica* rapidly toggles effector secretion and can resume cell division in response to changing external conditions. *Front. Microbiol.* **10**, 2128 (2019).
48. S. R. Shames, L. Liu, J. C. Havey, W. B. Schofield, A. L. Goodman, C. R. Roy, Multiple *Legionella pneumophila* effector virulence phenotypes revealed through high-throughput analysis of targeted mutant libraries. *Proc. Natl. Acad. Sci. U.S.A.* **114**, E10446–E10454 (2017).
49. A. Takaya, T. Tomoyasu, H. Matsui, T. Yamamoto, The DnaK/DnaJ chaperone machinery of *Salmonella enterica* Serovar typhimurium is essential for invasion of epithelial cells and survival within macrophages, leading to systemic infection. *Infect. Immun.* **72**, 1364–1373 (2004).
50. W. Shi, Y. Zhou, J. Wild, J. Adler, C. A. Gross, DnaK, DnaJ, and GrpE are required for flagellum synthesis in *Escherichia coli*. *J. Bacteriol.* **174**, 6256–6263 (1992).
51. L. A. Kelley, S. Mezulis, C. M. Yates, M. N. Wass, M. J. E. Sternberg, The Phyre2 web portal for protein modeling, prediction and analysis. *Nat. Protoc.* **10**, 845–858 (2015).
52. A. Roy, A. Kucukural, Y. Zhang, I-TASSER: A unified platform for automated protein structure and function prediction. *Nat. Protoc.* **5**, 725–738 (2010).
53. A. Satoh, L. Stein, S. Imai, The role of mammalian sirtuins in the regulation of metabolism, aging, and longevity, in *Histone Deacetylases: The Biology and Clinical Implication*, T.-P. Yao, E. Seto Eds. (Springer Berlin Heidelberg, 2011), vol. 206, pp. 125–162.
54. B. R. Kelley, J. C. Ellis, A. Large, L. G. Schneider, D. Jacobson, J. G. Johnson, Whole-genome sequencing and bioinformatic analysis of environmental, agricultural, and human *Campylobacter jejuni* isolates from East Tennessee. *Front. Microbiol.* **11**, 571064 (2020).
55. S. Moniot, M. Weyand, C. Steegborn, Structures, substrates, and regulators of mammalian sirtuins – Opportunities and challenges for drug development. *Front. Pharmacol.* **3**, 16 (2012).
56. S. Imai, L. Guarente, NAD^+ and sirtuins in aging and disease. *Trends Cell Biol.* **24**, 464–471 (2014).
57. J. E. Christensen, S. A. Pacheco, M. E. Konkel, Identification of a *Campylobacter jejuni* -secreted protein required for maximal invasion of host cells. *Mol. Microbiol.* **73**, 650–662 (2009).
58. M. E. Konkel, J. D. Klena, V. Rivera-Amill, M. R. Monteville, D. Biswas, B. Raphael, J. Mickelson, Secretion of virulence proteins from *Campylobacter jejuni* is dependent on a functional flagellar export apparatus. *J. Bacteriol.* **186**, 3296–3303 (2004).
59. A. M. Barrero-Tobon, D. R. Hendrixson, Flagellar biosynthesis exerts temporal regulation of secretion of specific *Campylobacter jejuni* colonization and virulence determinants. *Mol. Microbiol.* **93**, 957–974 (2014).
60. S. Chakravarthy, B. Huot, B. H. Kvitko, Effector translocation: Cya reporter assay, in *Bacterial Protein Secretion Systems,* Eds. L. Journet, E. Cascales, (Springer New York, 2017), vol. 1615, pp. 473–487.

61. J. G. Johnson, J. A. Gaddy, V. J. DiRita, The PAS domain-containing protein HeuR regulates heme uptake in *Campylobacter jejuni*. *MBio* **7**, e01691-16 (2016).
62. M. E. Konkel, B. J. Kim, V. Rivera-Amill, S. G. Garvis, Bacterial secreted proteins are required for the internalization of *Campylobacter jejuni* into cultured mammalian cells. *Mol. Microbiol.* **32**, 691–701 (1999).
63. S.-I. Aizawa, Bacterial flagella and type III secretion systems. *FEMS Microbiol. Lett.* **202**, 157–164 (2001).
64. J. M. Neal-McKinney, M. E. Konkel, The *Campylobacter jejuni* CiaC virulence protein is secreted from the flagellum and delivered to the cytosol of host cells. *Front. Cell. Infect. Microbiol.* **2**, 31 (2012).
65. B. C. Russo, J. K. Duncan-Lowey, P. Chen, M. B. Goldberg, The type 3 secretion system requires actin polymerization to open translocon pores. *PLOS Pathog.* **17**, e1009932 (2021).
66. E. F. Kenny, A. Herzig, R. Krüger, A. Muth, S. Mondal, P. R. Thompson, V. Brinkmann, H. von Bernuth, A. Zychlinsky, Diverse stimuli engage different neutrophil extracellular trap pathways. *eLife* **6**, e24437 (2017).
67. S. L. Lebeis, K. R. Powell, D. Merlin, M. A. Sherman, D. Kalman, Interleukin-1 receptor signaling protects mice from lethal intestinal damage caused by the attaching and effacing pathogen *Citrobacter rodentium*. *Infect. Immun.* **77**, 604–614 (2009).
68. D. Chen, S. L. McKune, N. Singh, J. Y. Hassen, W. Gebreyes, M. J. Manary, K. Bardosh, Y. Yang, N. Diaz, A. Mohammed, Y. Terefe, K. T. Roba, M. Ketema, N. Ameha, N. Assefa, G. Rajashekara, L. Deblais, M. Ghanem, G. Yimer, A. H. Havelaar, *Campylobacter* colonization, environmental enteric dysfunction, stunting, and associated risk factors among young children in rural Ethiopia: A cross-sectional study from the Campylobacter Genomics and Environmental Enteric Dysfunction (CAGED) project. *Front. Public Health* **8**, 615793 (2021).
69. F. Ren, X. Li, H. Tang, Q. Jiang, X. Yun, L. Fang, P. Huang, Y. Tang, Q. Li, J. Huang, X.-A. Jiao, Insights into the impact of flhF inactivation on *Campylobacter jejuni* colonization of chick and mice gut. *BMC Microbiol.* **18**, 149 (2018).
70. A. Gupta, M. Bansal, B. Wagle, X. Sun, N. Rath, A. Donoghue, A. Upadhyay, Sodium butyrate reduces *Salmonella enteritidis* infection of chicken enterocytes and expression of inflammatory host genes in vitro. *Front. Microbiol.* **11**, 553670 (2020).
71. F. Rivera-Chávez, L. F. Zhang, F. Faber, C. A. Lopez, M. X. Byndloss, E. E. Olsan, G. Xu, E. M. Velazquez, C. B. Lebrilla, S. E. Winter, A. J. Bäumler, Depletion of butyrate-producing clostridia from the gut microbiota drives an aerobic luminal expansion of salmonella. *Cell Host Microbe* **19**, 443–454 (2016).
72. H. Xiong, B. Guo, Z. Gan, D. Song, Z. Lu, H. Yi, Y. Wu, Y. Wang, H. Du, Butyrate upregulates endogenous host defense peptides to enhance disease resistance in piglets via histone deacetylase inhibition. *Sci. Rep.* **6**, 27070 (2016).
73. I. Ahmed, K. Yusuf, B. C. Roy, J. Stubbs, S. Anant, T. M. Attard, V. Sampath, S. Umar, Dietary interventions ameliorate infectious colitis by restoring the microbiome and promoting stem cell proliferation in mice. *Int. J. Mol. Sci.* **23**, 339 (2022).
74. J. A. Jiminez, T. C. Uwiera, D. W. Abbott, R. R. E. Uwiera, G. D. Inglis, Butyrate supplementation at high concentrations alters enteric bacterial communities and reduces intestinal inflammation in mice infected with *Citrobacter rodentium*. *mSphere* **2**, e00243-17 (2017).
75. J. W. Park, H. Y. Kim, M. G. Kim, S. Jeong, C.-H. Yun, S. H. Han, Short-chain fatty acids inhibit staphylococcal lipoprotein-induced nitric oxide production in murine macrophages. *Immune Netw.* **19**, e9 (2019).
76. S. Traisaeng, D. R. Herr, H.-J. Kao, T.-H. Chuang, C.-M. Huang, A derivative of butyric acid, the fermentation metabolite of *Staphylococcus epidermidis*, inhibits the growth of a *Staphylococcus aureus* strain isolated from atopic dermatitis patients. *Toxins* **11**, 311 (2019).
77. M. Mombelli, J. Lugrin, I. Rubino, A.L. Chanson, M. Giddey, T. Calandra, T. Roger, Histone deacetylase inhibitors impair antibacterial defenses of macrophages. *J. Infect. Dis.* **204**, 1367–1441 (2011).
78. A.M. Grabiec, J. Potempa, Epigenetic regulation in bacterial infections: targeting histone deacetylases. *Crit. Rev. Microbiol* **44**, 336–686 (2018).
79. B. E. Bernstein, E. L. Humphrey, R. L. Erlich, R. Schneider, P. Bouman, J. S. Liu, T. Kouzarides, S. L. Schreiber, Methylation of histone H3 Lys 4 in coding regions of active genes. *Proc. Natl. Acad. Sci. U.S.A.* **99**, 8695–8700 (2002).
80. H.-Y. Ryu, M. Hochstrasser, Histone sumoylation and chromatin dynamics. *Nucleic Acids Res.* **49**, 6043–6052 (2021).
81. W. D. Zencheck, H. Xia, L. M. Weiss, Lysine post-translational modifications and the cytoskeleton. *Essays Biochem.* **52**, 135–145 (2012).
82. X. Zhang, B. Li, A. H. Rezaeian, X. Xu, P.-C. Chou, G. Jin, F. Han, B.-S. Pan, C.-Y. Wang, J. Long, A. Zhang, C.-Y. Huang, F.-J. Tsai, C.-H. Tsai, C. Logothetis, H.-K. Lin, H3 ubiquitination by NEDD4 regulates H3 acetylation and tumorigenesis. *Nat. Commun.* **8**, 14799 (2017).
83. P. Saha, B. S. Yeoh, X. Xiao, R. M. Golonka, V. Singh, Y. Wang, M. Vijay-Kumar, PAD4-dependent NETs generation are indispensable for intestinal clearance of *Citrobacter rodentium*. *Mucosal Immunol.* **12**, 761–771 (2019).
84. H. P. Gideon, J. Phuah, B. A. Junecko, J. T. Mattila, Neutrophils express pro- and anti-inflammatory cytokines in granulomas from *Mycobacterium tuberculosis*-infected cynomolgus macaques. *Mucosal Immunol.* **12**, 1370–1381 (2019).
85. C. Tecchio, A. Micheletti, M. A. Cassatella, Neutrophil-derived cytokines: Facts beyond expression. *Front. Immunol.* **5**, 508 (2014).
86. H. Li, Y. Li, C. Song, Y. Hu, M. Dai, B. Liu, P. Pan, Neutrophil extracellular traps augmented alveolar macrophage pyroptosis via AIM2 inflammasome activation in LPS-induced ALI/ARDS. *J. Inflamm. Res.* **14**, 4839–4858 (2021).
87. A. J. Monteith, J. M. Miller, C. N. Maxwell, W. J. Chazin, E. P. Skaar, Neutrophil extracellular traps enhance macrophage killing of bacterial pathogens. *Sci. Adv.* **7**, eabj2101 (2021).
88. T.-D. Tsourouktsoglou, A. Warnatsch, M. Ioannou, D. Hoving, Q. Wang, V. Papayannopoulos, Histones, DNA, and citrullination promote neutrophil extracellular trap inflammation by regulating the localization and activation of TLR4. *Cell Rep.* **31**, 107602 (2020).
89. A. Mangold, T. M. Hofbauer, A. S. Ondracek, T. Artner, T. Scherz, W. S. Speidl, K. A. Krychtiuk, R. Sadushi-Kolici, J. Jakowitsch, I. M. Lang, Neutrophil extracellular traps and monocyte subsets at the culprit lesion site of myocardial infarction patients. *Sci. Rep.* **9**, 16304 (2019).
90. Z. Parackova, I. Zentsova, P. Vrabcova, A. Klocperk, Z. Sumnik, S. Pruhova, L. Petruzelkova, R. Hasler, A. Sediva, Neutrophil extracellular trap induced dendritic cell activation leads to Th1 polarization in type 1 diabetes. *Front. Immunol.* **11**, 661 (2020).
91. C. E. M. Aarts, I. H. Hiemstra, A. T. J. Tool, T. K. van den Berg, E. Mul, R. van Bruggen, T. W. Kuijpers, Neutrophils as suppressors of T cell proliferation: Does age matter? *Front. Immunol.* **10**, 2144 (2019).
92. D. A. Dorward, C. D. Lucas, A. L. Alessandri, J. A. Marwick, F. Rossi, I. Dransfield, C. Haslett, K. Dhaliwal, A. G. Rossi, Technical advance: Autofluorescence-based sorting: Rapid and nonperturbing isolation of ultrapure neutrophils to determine cytokine production. *J. Leukoc. Biol.* **94**, 193–202 (2013).
93. S. M. Callahan, J. G. Johnson, Transposon-based identification of factors that promote *Campylobacter jejuni* nuclease activity. *Curr. Protoc.* **1**, e293 (2021).
94. D. R. Hendrixson, V. J. DiRita, Transcription of σ54-dependent but not σ28-dependent flagellar genes in *Campylobacter jejuni* is associated with formation of the flagellar secretory apparatus. *Mol. Microbiol.* **50**, 687–702 (2003).
95. B. R. Kelley, S. M. Callahan, J. G. Johnson, Transcription of cystathionine β-lyase (MetC) is repressed by HeuR in *Campylobacter jejuni*, and methionine biosynthesis facilitates colonocyte invasion. *J. Bacteriol.* **203**, e0016421 (2021).
96. S. M. Callahan, T. J. Hancock, J. G. Johnson, Characterization of *Campylobacter jejuni*–neutrophil interactions. *Curr. Protoc.* **1**, e294 (2021).
97. R. Akhtar, Z. Chaudhary, Y. He, Modified method for isolation of peripheral blood neutrophils from bovines and humans. *Int. J. Agro Vet. Med. Sci.* **4**, 8 (2010).
98. M.-P. Sory, G. R. Cornelis, Translocation of a hybrid YopE-adenylate cyclase from *Yersinia enterocolitica* into HeLa cells. *Mol. Microbiol.* **14**, 583–594 (1994).
99. O. Zharkova, S. H. Tay, H. Y. Lee, T. Shubhita, W. Y. Ong, A. Lateef, P. A. MacAry, L. H. K. Lim, J. E. Connolly, A.-M. Fairhurst, A flow cytometry-based assay for high-throughput detection and quantification of neutrophil extracellular traps in mixed cell populations. *Cytometry A* **95**, 268–278 (2019).
100. V. Brinkmann, B. Laube, U. Abu Abed, C. Goosmann, A. Zychlinsky, Neutrophil extracellular traps: How to generate and visualize them. *J. Vis. Exp.*, 1724 (2010).
101. E. A. Greenfield, *Antibodies: A Laboratory Manual* (Cold Spring Harbor Laboratory Press, 2014).
102. V. Brinkmann, U. Abu Abed, C. Goosmann, A. Zychlinsky, Immunodetection of NETs in paraffin-embedded tissue. *Front. Immunol.* **7**, 513 (2016).
103. R. S. Doster, J. A. Sutton, L. M. Rogers, D. M. Aronoff, J. A. Gaddy, *Streptococcus agalactiae* induces placental macrophages to release extracellular traps loaded with tissue remodeling enzymes via an oxidative burst-dependent mechanism. *MBio* **9**, e02084-18 (2018).
104. C. T. D. Price, H. E. Hanford, A. Vashishta, M. Ozanic, M. Santic, S. Uriarte, Y. A. Kwaik, Dot/Icm-dependent restriction of Legionella pneumophila within neutrophils. *mBio* **12**, e0100821 (2021).

Acknowledgments: We would like to thank D. Hendrixson at UT Southwestern for supplying the *C. jejuni* 81-176 *flgE* mutant and the RpoA antibody. We would also like to thank C. Price and Y. A. Kwaik at the University of Louisville for supplying the *ankB-cyaA* adenylate cyclase plasmid. We would also like to thank A. Monteith for reviewing the manuscript and providing comments. Last, we would like to thank M. Bunch, S. Sambrook, and J. Kolape for imaging of *C. jejuni*–induced murine NETs. **Funding:** Research was supported by UTK Start-Up Funds to J.G.J., USDA NIFA (2019-67017-29261) to J.G.J., NIH R01AI166535 to J.G.J., NIH K08AAI151100 to R.S.D., VA

Merit Award I01 BX005352-01 to J.A.G., and NIH R01HD090061 to J.A.G. **Author contributions:** Conceptualization: S.M.C. and J.G.J. Methodology: S.M.C. and J.G.J. Investigation: S.M.C., T.J.H, R.S.D., and J.G.J. Writing–original draft: S.M.C. and J.G.J. Writing–review and editing: S.M.C., T.J.H., R.S.D., C.B.P., M.E.W., J.A.G., and J.G.J. Funding acquisition: R.S.D., J.A.G., and J.G.J. Resources: J.A.G. and J.G.J. Supervision: J.G.J. **Competing interests:** The authors declare that they have no competing interests. **Data and materials availability:** All data needed to evaluate the conclusions in the paper are present in the paper and/or the Supplementary Materials. The strains can be provided by J.G.J. pending scientific review and a completed material transfer agreement. Requests for the strains should be submitted to J.G.J.

Submitted 4 August 2022
Accepted 13 July 2023
Published 11 August 2023
10.1126/sciadv.ade2693